AEDC-TR-77-56

AFOSR-TR-77-0749

cy.2

AN EXPERIMENTAL INVESTIGATION OF DUCTED,

REACTIVE, TURBULENT JET MIXING WITH RECIRCULATION

Chriss

ENGINE TEST FACILITY
ARNOLD ENGINEERING DEVELOPMENT CENTER
AIR FORCE SYSTEMS COMMAND
ARNOLD AIR FORCE STATION, TENNESSEE 37389

September 1977

Final Report for Period February 26 - October 26, 1976

Prepared for

AIR FORCE OFFICE OF SCIENTIFIC RESEARCH
BOLLING AIR FORCE BASE
WASHINGTON, D.C. 20332

NOTICES

When U. S. Government drawings specifications, or other data are used for any purpose other than a definitely related Government procurement operation, the Government thereby incurs no responsibility nor any obligation whatsoever, and the fact that the Government may have formulated, furnished, or in any way supplied the said drawings, specifications, or other data, is not to be regarded by implication or otherwise, or in any manner licensing the holder or any other person or corporation, or conveying any rights or permission to manufacture, use, or sell any patented invention that may in any way be related thereto.

Qualified users may obtain copies of this report from the Defense Documentation Center.

References to named commercial products in this report are not to be considered in any sense as an endorsement of the product by the United States Air Force or the Government.

This report has been reviewed by the Information Office (OI) and is releasable to the National Technical Information Service (NTIS). At NTIS, it will be available to the general public, including foreign nations.

APPROVAL STATEMENT

This technical report has been reviewed and is approved for publication.

FOR THE COMMANDER

MARION L. LASTER
Director of Test Engineering
Deputy for Operations

ALAN L. DEVEREAUX
Colonel, USAF
Deputy for Operations

REPORT DOCUMENTATION PAGE		READ INSTRUCTIONS BEFORE COMPLETING FORM
1 REPORT NUMBER AEDC-TR-77-56 AFOSR-TR-77-0749	2 GOVT ACCESSION NO.	3 RECIPIENT'S CATALOG NUMBER
4 TITLE (and Subtitle) AN EXPERIMENTAL INVESTIGATION OF DUCTED, REACTIVE, TURBULENT JET MIXING WITH RECIRCULATION		5 TYPE OF REPORT & PERIOD COVERED Final Report – February 26 – October 26, 1976
		6 PERFORMING ORG. REPORT NUMBER
7 AUTHOR(s) D. E. Chriss – ARO, Inc.		8 CONTRACT OR GRANT NUMBER(s)
9 PERFORMING ORGANIZATION NAME AND ADDRESS Arnold Engineering Development Center Air Force Systems Command Arnold Air Force Station, Tennessee 37389		10 PROGRAM ELEMENT, PROJECT, TASK AREA & WORK UNIT NUMBERS Program Element 61102F
11 CONTROLLING OFFICE NAME AND ADDRESS Arnold Engineering Development Center (XRFIS), Arnold Air Force Station, Tennessee 37389		12. REPORT DATE September 1977
		13. NUMBER OF PAGES 45
14 MONITORING AGENCY NAME & ADDRESS(if different from Controlling Office)		15 SECURITY CLASS. (of this report) UNCLASSIFIED
		15a. DECLASSIFICATION/DOWNGRADING SCHEDULE N/A

16 DISTRIBUTION STATEMENT (of this Report)

Approved for public release; distribution unlimited.

17. DISTRIBUTION STATEMENT (of the abstract entered in Block 20, if different from Report)

18 SUPPLEMENTARY NOTES

Available in DDC

19 KEY WORDS (Continue on reverse side if necessary and identify by block number)

jet mixing flow
gas flow
recirculation
turbulent mixing

mathematical analysis
experimental data

20 ABSTRACT (Continue on reverse side if necessary and identify by block number)

An experimental investigation of ducted, two stream, subsonic, reactive, turbulent jet mixing with recirculation was conducted. A primary jet of air at a mass flow rate of 0.075 lb/sec and velocity of 700 ft/sec was surrounded by an outer, low velocity, hydrogen stream. Data were obtained with hydrogen-air ratios of 0.143 and 0.107. The duct-to-inner nozzle diameter ratio was ten. Radial distributions of hydrogen mass fraction, mean axial velocity,

DD FORM 1473 1 JAN 73 EDITION OF 1 NOV 65 IS OBSOLETE

20. ABSTRACT (Continued)

turbulence intensity, and total pressure as well as axial distri-
butions of wall hydrogen mass fraction and wall static pressure
are presented for axial stations from one-half to five duct
diameters from the nozzle exit plane. Comparison of the experi-
mental data with calculations assuming frozen or equilibrium
chemistry indicate that the measured velocity, pressure, and
composition data are, in general, self-consistent. The maximum
turbulent intensities which occurred in the center of the mixing
layer and within the recirculation eddy were very high having
values of 20 percent of the jet exit velocity. The velocity and
composition field indicate that, while the mixing in the reactive
flow field is slower than for the nonreactive case, the reaction
had little effect on the size and location of the recirculation
zone within the mixing duct.

AFSC
Arnold AFS Tenn

PREFACE

CONTENTS

ILLUSTRATIONS

TABLES

APPENDIXES

1.0 INTRODUCTION

Recirculating flow fields established by turbulent jet mixing of two coaxial streams in a constant-area, axisymmetric duct occur in many industrial and aerospace burner, furnace, and combustor configurations. The so-called "sudden" expansion or "dump" combustors used in ramjet-rocket propulsion systems are designed on the principle of establishing and maintaining combustion in regions of recirculating flow within the combustor.

The purpose of the study reported herein was to obtain data to aid in the development of analytical techniques to analyze and predict the turbulent mixing and combustion phenomena which occur in a wide variety of engineering applications. The development and evaluation of analytical techniques require data on many different flow configurations if the techniques are to be general and applicable to more than a limited number of configurations. Experimental data are available for boundary-layer-type flow but development and evaluation of analytical models for ducted recirculating flow configurations has been hampered by the lack of detailed experimental flow field information for such configurations.

Data were obtained in a configuration similar to that of a "dump" combustor. The apparatus is the same used in the work reported by Schulz (Ref. 1) which was concerned with nonreacting, variable-density, confined, axisymmetric recirculating flows. The objective of the present study was to obtain total pressure, mean axial velocity, turbulence intensity, gas composition, and wall static pressure distributions in a reacting, confined, axisymmetric, recirculating flow field for two secondary-to-primary flow ratios. The data may be used as a guide for design estimates for combustors or combustion processes and to aid in developing and evaluating theoretical models and predictive techniques for such flows and processes. The data are tabulated in Appendix A for the convenience of other investigators.

The essential features of the recirculating flow field are shown in Fig. 1. For a certain range of fluid influx conditions, jet mixing of coaxial streams leads to the creation of an eddy of recirculating fluid existing on a time-averaged basis as a torodial, highly vortical region with high turbulent intensities and relatively low average velocities. The eddy of the recirculating region is generated when the "entrainment or pumping capacity" of the higher velocity primary jet stream is greater than the mass flow available in the outer, lower velocity secondary stream. For those conditions, the-primary jet "establishes" the recirculation eddy which provides mass flux to balance the jet entrainment requirements. The recirculation eddy can exist with or without secondary flow. However, as the secondary mass ·flow rate is increased to some critical "blow-off"

value with a constant primary jet mass flow rate, the recirculation eddy structure disappears and the duct flow will be characterized by positive axial velocities throughout the flow. The pertinent features which may be used to describe the time-averaged flow field with recirculation are:

1. The axial location of the characteristic time-averaged stagnation points on the duct wall, denoted X_{FS} and X_{RS} in Fig. 1.

2. The time-averaged axial velocity field.

3. The time-averaged distribution of mass, energy, or temperature of the fluid from the primary stream which characterizes the qualitative and quantitative nature of the mixing that has occurred between the two streams.

4. The time-averaged axial distribution of wall static pressure.

All of these gross features of the flow, their spatial distributions and magnitudes, appear from experimental evidence to be dependent on the ratios (u_s/u_p, ρ_s/ρ_p, R_s/R_p), a Reynolds number based on the primary flow at the nozzle exit station, and on chemical reactions occurring in the flow. However, it is also an empirical observation that for sufficiently high values ($> 1.5 \times 10^4$) of the primary jet Reynolds number, defined by

$$N_{Re_P} = \rho_p u_p R_p / \mu_p \qquad (1)$$

the time-averaged velocity, species concentration, and static pressure fields become independent of N_{Re}, which is the case in the present study.

2.0 APPARATUS

2.1 TEST CELL

The test cell used is identical to the one described in Ref. 1 except for the 1/4-in. slot shown in Fig. 2. The slot provided optical access to allow the use of a laser velocimeter. A quartz window was used to seal the slot. The test chamber consisted of a 5-ft-long stainless steel duct with an inside diameter of 5.24 in. A mechanically driven axially traversing nozzle assembly was mounted inside the duct. The nozzle assembly was traversed in discrete steps during the testing to vary the distance between the primary jet nozzle exit plane and the radially positionable pitot pressure and gas sampling probe. An O-ring system provided a seal between the movable nozzle assembly and the duct.

The nozzle assembly included a circular, 0.524-in.-diam nozzle (Fig. 3), which introduced the primary air jet at 700 ft/sec, and an annular secondary injector assembly, through which hydrogen entered the duct. The duct-to-primary jet diameter ratio was ten. The secondary hydrogen flow passed through two porous plates and a screen pack shown in Fig. 2, which acted to stabilize the flow system.

External water spray nozzles were positioned outside the duct to cool the walls. A spark plug was located downstream of the traversing probe to ignite the combustible hydrogen-air mixture.

2.2 INSTRUMENTATION

2.2.1 Pressure and Temperature

A water-cooled total pressure and gas sampling probe of the type discussed in Ref. 2 was installed in the duct at a fixed axial position. The probe tip, detailed in Fig. 4, was traversed radially across the duct by a hydraulic drive mechanism. By combination of the motion of the axial traversing nozzle assembly and the radially traversing probe, axial and radial surveys were made in the recirculating flow field. The total pressure was sensed with a variable capacitance transducer and a strain-gage transducer to obtain maximum accuracy over the wide range of pressure encountered.

In addition to the probe assembly, 41 static pressure orifices (0.040-in.-diam) were installed approximately one inch apart along the duct wall. Five of the orifices were used to obtain gas samples, and the remaining 36 were connected to a water manometer which was photographed during the tests to record the wall static pressure distribution.

The total temperature of the gaseous supplies of air and hydrogen was measured with copper-constantan thermocouples upstream of critical-flow venturis, which were used to meter the primary and secondary mass flows.

2.2.2 Gas Concentration

The molecular weight of gas samples was measured using gas-sample-driven fluidic oscillators. The theory and use of fluidic oscillator systems to measure gas composition is described in Refs. 2, 3, and 4. The output frequency of a fluidic oscillator depends on the speed of sound of the gas sample passing through the oscillator, the oscillator configuration, and the pressure drop across the oscillator. However, through temperature control and calibration, the oscillator frequency can be established as a function only of the molecular weight and specific heat ratio of the gas sample passing through the oscillator.

The fluidic oscillator system consisted of six oscillators mounted in a steam-filled box for temperature control. Consistent operation of the oscillator system was ensured by analyzing an air sample during each data cycle. Calibration of the system was accomplished using gas samples of air, helium, and mixtures of nitrogen and hydrogen having a range of molecular weights between 6 and 20. The calibration curves were supplemented by the fully mixed and reacted composition of the two test gas mixtures. The effect of specific heat ratio could be neglected because the system was calibrated with gaseous mixtures whose specific heat ratios were essentially the same as the mixtures being measured.

Each time composition data were obtained with the traversing probe, data were also obtained from each of the five wall orifices connected to the gas analyzer. The location of each orifice relative to the nozzle exit depends on the axial location of the nozzle. By taking data at several nozzle locations a rather complete axial variation of composition along the wall was obtained. At each nozzle location, data were recorded for each probe position so that there are 8- to 15 samples per orifice for each nozzle position. The data presented are average values of hydrogen mass fraction with the outliers eliminated by Thompson's τ technique (Ref. 5).

2.2.3 Laser Velocimeter

Velocity measurements were made in the duct with a two-component, Bragg-diffracted laser velocimeter (LV) shown in Fig. 5 and described in Ref. 6. However, in the present study, only the axial velocity component was obtained. Light from the 514.5-nm line of an argon-ion laser is focused and directed through an ultrasonically driven Bragg cell which diffracts the incident radiation into several nearly equal intensity beams. Two of the beams are passed by a beam stop and refocused to a point in the flow field. In this probe volume, a set of interference fringes is formed. Since the Bragg cell shifts the frequency of each of the transmitted beams, the fringes are not stationary but move at a reference velocity proportional to the frequency of the ultrasonic drivers. Velocities, accordingly, are determined relative to the reference velocity so that the directional ambiguity inherent in most LV systems is avoided.

Light scattered from particles passing through the probe volume is received by a photomultiplier tube (PMT) through the collector optics. By viewing the probe volume through an aperture at an off-axis collection angle, the effective probe volume can be varied. The collector optics were positioned so that operation was in the back scatter mode.

The signal received by the PMT was amplified and filtered by the signal-conditioning electronics to enhance its signal-to-noise ratio. The resulting signals were processed by the

Doppler Data Processors to determine the period of the Doppler shift. From the period of the signal, the reference frequency of the Bragg drivers, and the known characteristics of the input optics, the velocity of the particles may be determined. The system had the capability to measure axial velocities from -115 to 700 ft/sec.

In some flows, natural seeding may be adequate for making laser velocimeter measurements. However, at the temperatures in the reacting flow field, not enough natural particles survive to make velocity measurements within a reasonable time period. Thus, a particle seeding device was developed with which the primary air stream was seeded with one-micron alumina particles. However, it is likely that the actual particle sizes were larger than one micron because of aggregation of the particles (Ref. 7).

An operational problem was encountered in taking LV data through the slot in the cell wall. Water, formed in the combustion process, deposited on the quartz window surface. It was necessary to shield the viewing port area and heat the window surface to avoid condensation.

2.3 PRECISION OF MEASUREMENTS

The uncertainty of a measured parameter was determined from the bias limits and precision indices of the instrumentation by the procedures developed in Ref. 8. Given the bias limits and precision indices associated with the measurements necessary to define any parameter (Φ), the total uncertainty in Φ is defined as

$$U_\Phi = \pm (B_\Phi + t_{95} S_\Phi) \qquad (2)$$

where

$$B_\Phi = \sqrt{\sum_{i=1}^{N} \left[\left(\frac{\partial \Phi}{\partial \xi_i} \right) B_{\xi_i} \right]^2} \qquad (3)$$

is the bias limit for Φ, and

$$S_\Phi = \sqrt{\sum_{i=1}^{N} \left[\left(\frac{\partial \Phi}{\partial \xi_i} \right) S_{\xi_i} \right]^2} \qquad (4)$$

is the precision index for Φ, and ξ are the measured parameters which define Φ; that is,

$$\Phi = \Phi(\xi_i), \ i = 1, \ldots, N$$

and N is the number of measured parameters that define Φ. The parameter t_{95} is the "95 percentile point for the two-tailed students 't' distribution."

The bias limits and precision indices of instruments vary with the magnitude of measured quantities. Therefore, representative test conditions were selected upon which to base the precision indices and bias limits. Typical bias limits, precision indices, and uncertainties in the fundamental, measured parameters, the calculated velocities for frozen and equilibrium conditions, and the hydrogen gas concentrations, which are calculated from the fundamental, measured parameters, are presented in Table 1.

The uncertainties for the laser velocimeter measurements were calculated by the method outlined in Ref. 6, which was developed for the laser velocimeter used in these experiments. The uncertainty is ±4 percent of the measured value at -100 ft/sec and ±3 percent at 700 ft/sec.

2.4 TEST PROCEDURE

Calibration factors for the pressure and concentration instrumentation were determined before each test from application of a set of known pressures and molecular weights to each system. The sensitivity of each measurement system was obtained over ranges of values expected during the test. Temperature instrumentation was calibrated by the application of known voltages before each test. Data other than manometer pressures were recorded on seven-track, incremental, magnetic tape by a programmable Hewlett-Packard 2010 data acquisition system. The impact probe pressure was also displayed on an x-y recorder.

Prior to each test, the LV equipment was adjusted to obtained maximum power of the 514.5-nm spectral line, and the Bragg driver and Bragg cell were balanced to obtain equal intensities in the two unblocked beams. After the adjustments were completed, the fringe spacing and moving orientation with respect to the jet axis were determined. A detailed discussion of the procedure is presented in Ref. 6. A high-speed minicomputer data acquisition system was used to acquire the LV data.

At the beginning of each test, a vacuum check was performed to determine if there were any leaks in the pressure measuring system. A mixture of hydrogen and air in the test cell was ignited at very low flow rates. The flows were carefully increased together to avoid flame blow out. Conditions were set by establishing the desired flow rates of air and hydrogen as indicated by the pressure and temperatures upstream of the metering venturis. The LV and probe data (total pressure and gas composition) were taken during different test periods so that the probe would not perturb the flow field while the LV measurements were being made.

For probe data, the nozzle assembly was positioned at a desired distance from the probe. A continuous x-y plotter trace of total pressure versus radial position was taken to guide the selection of the radial locations to take total pressure and gas composition data. The probe was then incremented across the stream to obtain a profile.

To obtain LV data, the LV probe volume was positioned on the horizontal centerline of the test cell and then the laser velocimeter was traversed vertically to record data at prescribed increments. It was necessary to realign the LV with respect to the duct centerline each time the nozzle assembly was repositioned because of movement of the duct caused by the change in the location of the combustion region.

3.0 RESULTS AND DISCUSSION

Experimental data were obtained in a ducted, subsonic, axisymmetric, reacting, recirculating flow field with a primary jet airflow rate of 0.075 lb/sec and secondary outer stream hydrogen flow rates of 0.011 and 0.008 lb/sec. These flow rates result in fuel-air ratios (F/A) of 0.143 lb H_2/lb air and 0.107 lb H_2/lb air where the stoichiometric F/A ratio is 0.029 lb H_2/lb air. The static pressure in the duct was 13.8 psia. The measurements were made at axial stations from one-half to five duct diameters from the primary nozzle exit plane. The data include radial distributions of hydrogen mass fraction, mean axial velocity, axial turbulence intensity, and total pressure and axial distributions of wall hydrogen mass fraction and wall static pressure. The nominal test conditions are tabulated in Table 2 and the data are tabulated in Appendix A.

3.1 VELOCITY MEASUREMENTS

The radial distribution of mean axial velocity and axial turbulence intensity for the two fuel-air ratios are shown in Figs. 6 and 7. The data are nondimensionalized by the measured nominal primary jet exit velocity, 700 ft/sec.

The turbulence intensity (u'/u_p) for both fuel-air ratios has a maximum value of approximately 0.20 which, for X/D less than 3, occurs near the center of the mixing zone, i.e., where du/dr is a maximum. For X/D greater than 3, the turbulence intensity is approximately constant at 0.20 across the duct except for X/D = 5 at F/A = 0.107, which has an almost constant value of 0.11. The local turbulence intensity (u'/u) can be very high, having values of 100 percent or more of the local mean axial velocity when the local mean axial velocity is 150 ft/sec or less.
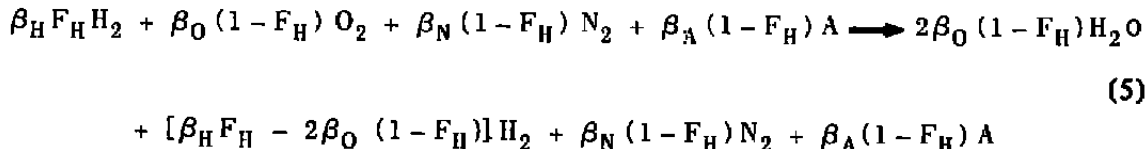
The decay of the mean axial velocity along the duct centerline is shown in Fig. 8. The velocity in the reactive cases decay less rapidly than the nonreactive case even in the near region (X/D = 1/2 and 1). It has been noted previously that the velocity in reactive

streams decays less rapidly than comparable nonreactive streams (Ref. 9), but a complete explanation for this phenomenon has not been given. It is recognized that, for constant area duct flow with mixing and heat addition, the average velocity in the duct must be higher than the nonreactive case for the same pressure and mass flow because of the higher temperature. However, the reason for the delayed decay of the potential core region in the reactive case, where neither mixing nor burning has taken place, is not obvious. The conventional X^{-1} decay for a free jet and the fully mixed equilibrium velocities are also shown in Fig. 8 for comparison purposes.

Figure 9 shows the location of the locus of points of zero mean axial velocity in the reactive recirculating flow field. The solid line was deduced from the data of Ref. 1 for the nonreactive recirculating case with F/A = 0.14. The Ref. 1 data were estimated from the results of pressure and composition measurements taken with forward and rearward facing pitot probes. The agreement is within the uncertainty of the measurements and indicates that the reaction has had little effect on the location of the recirculation zone.

3.2 HYDROGEN MASS FRACTION

For the reacting fuel-rich hydrogen-air mixture, the elemental hydrogen mass fraction (F_H) is related to the mixture molecular weight (W) through the general chemical relationship:

$$\beta_H F_H H_2 + \beta_O (1 - F_H) O_2 + \beta_N (1 - F_H) N_2 + \beta_A (1 - F_H) A \longrightarrow 2\beta_O (1 - F_H) H_2 O \tag{5}$$

$$+ [\beta_H F_H - 2\beta_O (1 - F_H)] H_2 + \beta_N (1 - F_H) N_2 + \beta_A (1 - F_H) A$$

By substituting the appropriate molecular weights, one obtains

$$F_H = \frac{2.1335}{W} - 0.05822 \tag{6}$$

The mixture molecular weight (W) is related to the frequency of the fluid oscillators. Note that the fully mixed value of F_H is equal to $(F/A)/[(F/A) + 1]$.

The radial distributions of F_H for F/A = 0.143 and F/A = 0.107 are shown in Figs. 10 and 11, respectively. As expected because of the mixing process, the centerline value of F_H increases and the wall value decreases with increasing axial distance from the primary nozzle exit plane. Note that no pure hydrogen was measured even at X/D = 0.5. However, recall that the velocity data (Fig. 9) indicate that X/D = 0.5 is close to the average location of the forward stagnation region. In addition, the lower values of F_H and the highly turbulent velocity field near the wall indicate that counterstream turbulent

diffusion of species apparently causes a dilution of the H_2 stream. The data at R/R_D = 0.2 in Fig. 10 for X/D = 2 and 3 indicate that the mixing is less rapid in the reactive than the nonreactive case which causes the dilution of the H_2 stream at X/D = 0.5 and 1.0 to be less in the reactive case.

The axial distribution of F_H along the duct wall (Fig. 12) also shows that, near the nozzle exit plane, F_H for the reactive case is higher than for the nonreactive data. The nonreactive F_H decays more rapidly than the reactive case which is consistent with the results of Fig. 10. The data also indicate that the upstream diffusion of species extends very near to the primary nozzle exit since F_H is less than unity in that region. The fully mixed value of F_H, calculated from the measured mass flows, shown in Fig. 12, is 0.128 for F/A = 0.143 and 0.096 for F/A = 0.107. For X/D near 5, the hydrogen mass fraction for F/A = 0.107 is lower than the data for F/A = 0.143 as would be expected. However, both data sets are below their fully mixed values.

3.3 PRESSURE DATA

The axial distribution of wall static pressure (shown in Fig. 13) is typical of distributions encountered in separated, reattached flows. The static pressure rise for the nonreactive recirculating flow is only slightly different in location from that of the reactive cases which is another indication that the chemical heat addition had little influence on the position of the recirculating zone. The radial distributions of total pressure are shown in Figs. 14 and 15.

3.4 VELOCITY CALCULATIONS-COMPARISON WITH MEASUREMENTS

The velocities measured with the laser velocimeter are compared with velocities calculated from the measured gas composition and pressures assuming either frozen or equilibrium chemistry. These two assumptions, about the state of the chemistry, provide upper and lower limits for the actual velocities in the flow field. Thus, by comparing the measured velocity with the computed velocity limits, one can infer the state of the reactions occurring in the gas. The static pressure measured on the duct wall at the axial location of the velocity measurements was used in the calculation along with the enthalpies of the inlet streams. The calculation procedure is described in Appendix B.

A comparison of measured and computed velocities is presented in Figs. 16 and 17. The LV velocity data at the first three axial stations (X/D = 1/2, 1, and 2) agree reasonably well with that calculated, assuming frozen conditions, especially on the centerline of the flow indicating that no reaction is taking place in that region. At station X/D = 3, the LV velocities agree more closely with velocities calculated at frozen conditions at the center, but agrees more closely with the velocities calculated from

equilibrium conditions near the wall. At station X/D = 4, the LV velocities in the recirculating zone, where reactions are expected, agree with the values calculated with the equilibrium assumption and indicate partial combustion elsewhere.

At station X/D = 5 with of F/A = 0.143, the LV velocities are higher than the velocities calculated for either frozen or equilibrium conditions. Particle dynamics calculations were made using a modified Stokes equation in a computer code developed by Hsieh (Ref. 10). The results indicate that the particle agglomoration could increase particle sizes to as much as two to five microns and give a difference between gas velocity and particle velocity of only 2 to 13 ft/sec, respectively, at X/D = 5. Therefore, it is not likely that particle lag is a significant factor in the velocity results. Most probably the discrepancy is caused by a combination of uncertainties in the calculated velocities caused by the small pressure differences (0.04 to 0.06 psi) and the measured hydrogen mass fraction being lower than the completely mixed value. At station X/D = 5 for F/A = 0.107, the LV velocities agree fairly well with the equilibrium velocities, indicating that combustion is almost complete. In general, the measured velocities agree with the values calculated from the measured pressure and composition data and the equilibrium assumption at locations where complete chemical reactions would be expected and with values calculated with the frozen assumption where reactions would not be expected, thus indicating that the measured quantities are self-consistent.

4.0 CONCLUSIONS

Ducted, subsonic, axisymmetric, reacting, recirculating flow experiments were conducted in a combustor with a duct diameter-to-inner nozzle diameter ratio of ten. A primary jet of air at a mass flow rate of 0.075 lb/sec was surrounded by an outer hydrogen stream to obtain fuel-air ratios of 0.143 and 0.107. Analysis of the data led to the following conclusions:

1. Comparison of the measured velocity with that calculated from measured pressure and composition data assuming frozen or equilibrium chemistry show that the measured velocity, pressure, and composition data are self-consistent.

2. The locus of zero mean velocity locations in the recirculating zone and the wall static pressure distribution for the reactive tests agree with those for nonreactive tests, which indicates that the reaction has little effect on the location of the recirculation zone.

3. The gases in a ducted, axisymmetric, reacting, recirculating flow mix more slowly than those in a nonreactive system of the same configuration and fuel-air ratio. The centerline decay of both concentration and velocity is less rapid and the radial distributions of concentration and velocity approach uniform profiles less rapidly for the same duct length in the reacting case.

4. The turbulence intensity based on the jet mean exit axial velocity, 700 ft/sec, has a maximum value of 0.20, which occurs in the mixing zone in the near field (X/D < 3). For stations downstream of X/D = 3, the turbulence intensity across the duct was approximately constant and equal to 0.20 except near the duct wall. In the lower velocity regions where the local axial velocity was 150 ft/sec or less, the local turbulence intensity was 100 percent or more of the mean local velocity.

5. The hydrogen mass fraction, velocity, and turbulent intensity profiles indicate that counter-stream turbulent diffusion is responsible for the dilution of the secondary hydrogen stream in the vicinity of the nozzle exit.

REFERENCES

1. Schulz, R. J. "An Investigation of Ducted, Two-Stream, Variable Density, Turbulent Jet Mixing with Recirculation." AEDC-TR-76-152 (ADA034537), AFOSR-TR-76-1087, January 1977.

2. Rhodes, R. P. "Probing Techniques for Use in High Temperature Reacting Flows." AEDC-TR-68-44 (AD829143), March 1968.

3. LeRoy, M. J., Jr., and Gorland, S. H. "Sensing Molecular Weights of Gases with a Fluidic Oscillator." NASA TMX-1939, 1974.

4. Riddlebaugh, S. M. "Use of the Fluidic Oscillator to Measure Fuel-Air Ratios of Combustion Gases." NASA TM X-3068, 1974.

5. Klautsch, R. E. "A Statistical Procedure for Improving the Precision of Data Acquired on a Digital Data Acquisition System." M. S. Thesis, The University of Tennessee, Knoxville, 1974.

6. Barnett, D. O. and Giel, T. V., Jr. "Laser Velocimeter Measurements in Moderately Heated Jet Flows." AEDC-TR-76-156 (ADA038283), April 1977.

7. Durst, F., Melling, A., and Whitelaw, J. H. <u>Principles and Practice of Laser-Doppler Anemometry.</u> Academic Press, London 1976.

8. Abernethy, R. B., et al., Pratt and Whitney Aircraft, and Thompson J. W., Jr., ARO, Inc. "Handbook-Uncertainty in Gas Turbine Measurements." AEDC-TR-73-5 (AD755356), February 1973.

9. Rhodes, R. P., Harsha, P. T., and Peters, C. E. "Turbulent Kinetic Energy Analysis of Hydrogen-Air Diffusion Flames." <u>Acta Astronautica,</u> Vol. 1, pp. 443-470, 1970.

10. Hsieh, T. "Analysis of Velocity Measurements about a Hemisphere-Cylinder Using a Laser Velocimeter." <u>Journal of Spacecraft and Rockets,</u> April 1976.

11. Osgerby, I. T. and Rhodes, R. P. "An Efficient Numerical Method for the Calculation of Chemical Equilibrium in the H/C/O/N/A System." AEDC-TR-71-256 (AD741825), April 1972.
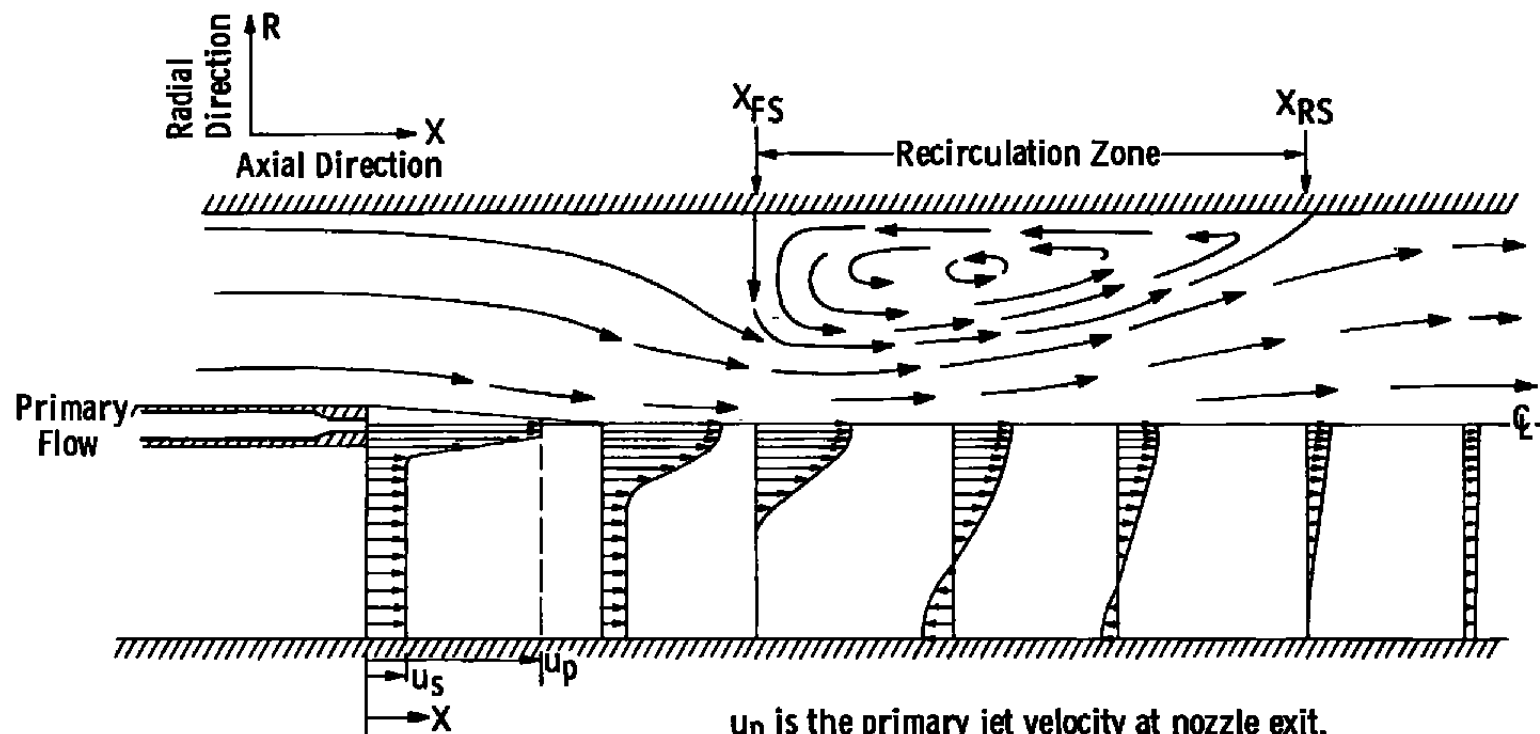
up is the primary jet velocity at nozzle exit.

us is the secondary jet velocity at nozzle exit.

Mean streamline pattern shown in upper half figure.

Mean axial velocity profiles shown in lower half figure.

Figure 1. Turbulent, ducted, mixing system with recirculation.

5.24-in. ID
Stainless
Steel Pipe

1/4-in. Wide Slot

O Rings

Probe

Flow

Baffle Plates
(Secondary Flow)

Primary Nozzle

Screen Pack

Flow

LV Beams

Window

Transmitting Lens
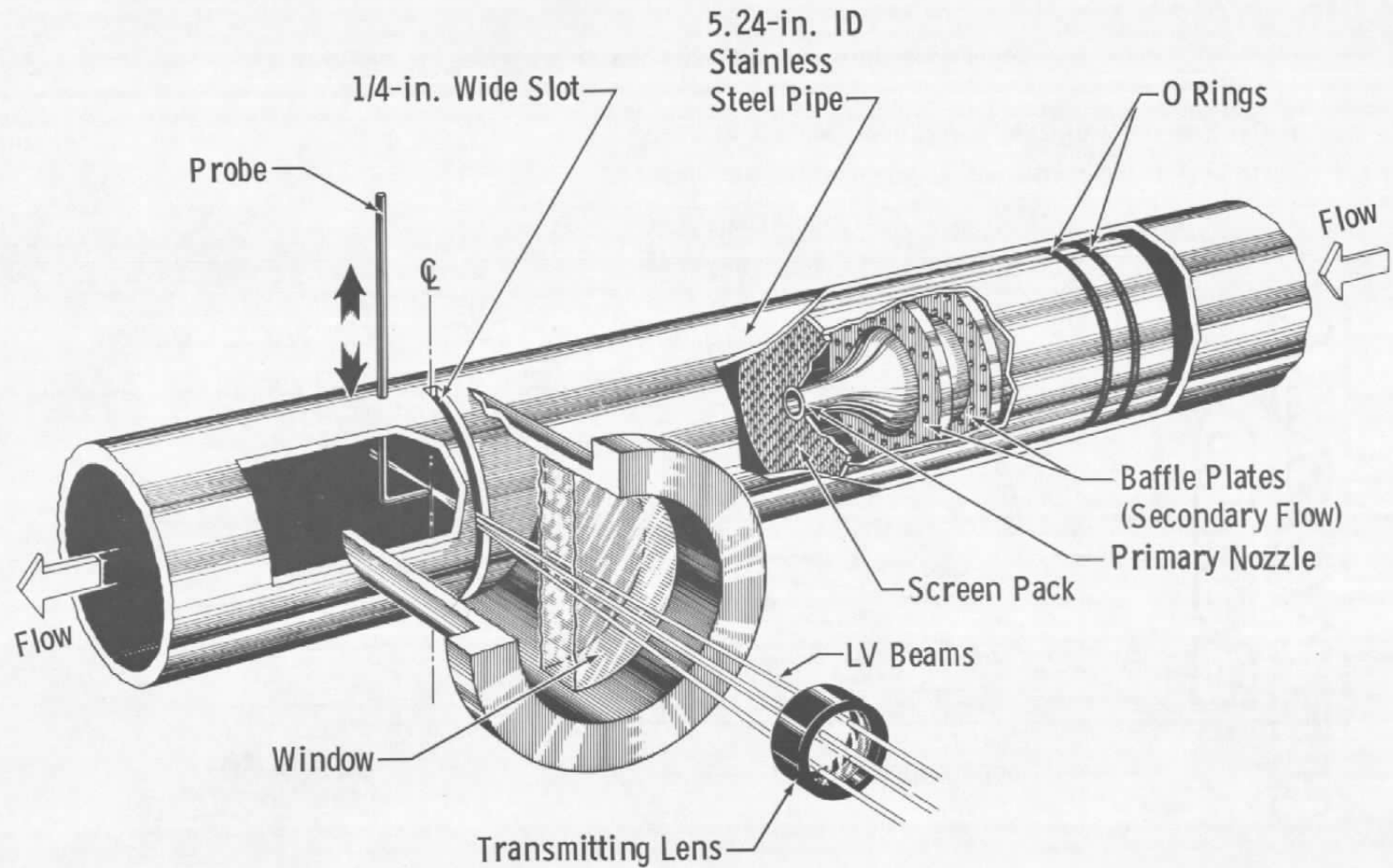
Figure 2. Recirculating flow combustor simulation facility.

All Dimensions in Inches
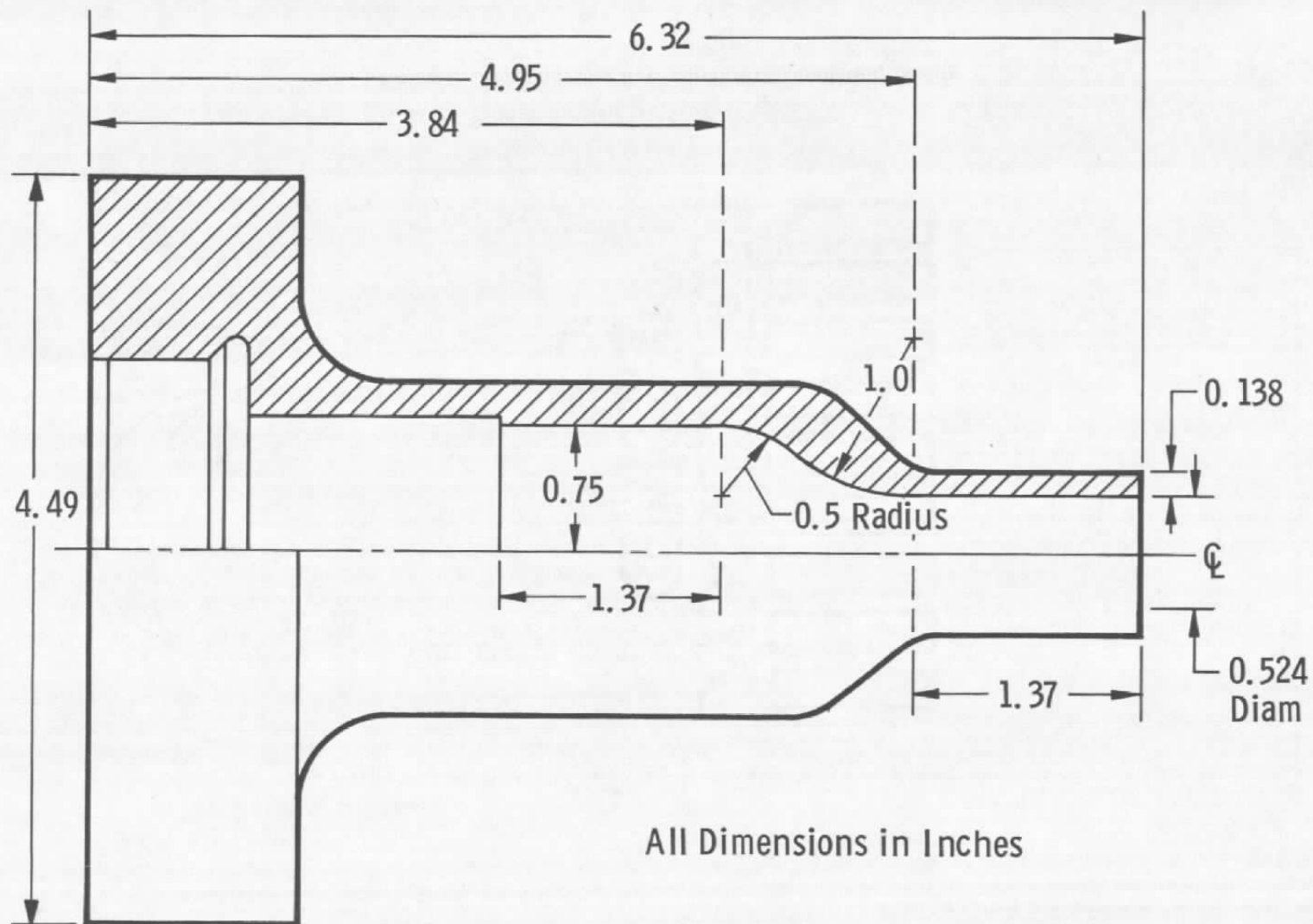
Figure 3. Primary flow nozzle assembly.

Notes: 1. Not to Scale

2. ⟵ Indicates Water Flow

1/4-in. Copper Tube

⟵ Demineralized Water Pressure, 350 psi

Heli-Arced Tip

0. 125-in. Diam by 0. 010-in. Wall Copper

0. 096-in. Diam by 0. 011-in. Wall Copper

0. 063-in. Diam by 0. 006-in. Wall Copper

Pitot Pressure and Gas Sampling Tube

Silver Solder

0. 02-in. -diam Drill

2 in.
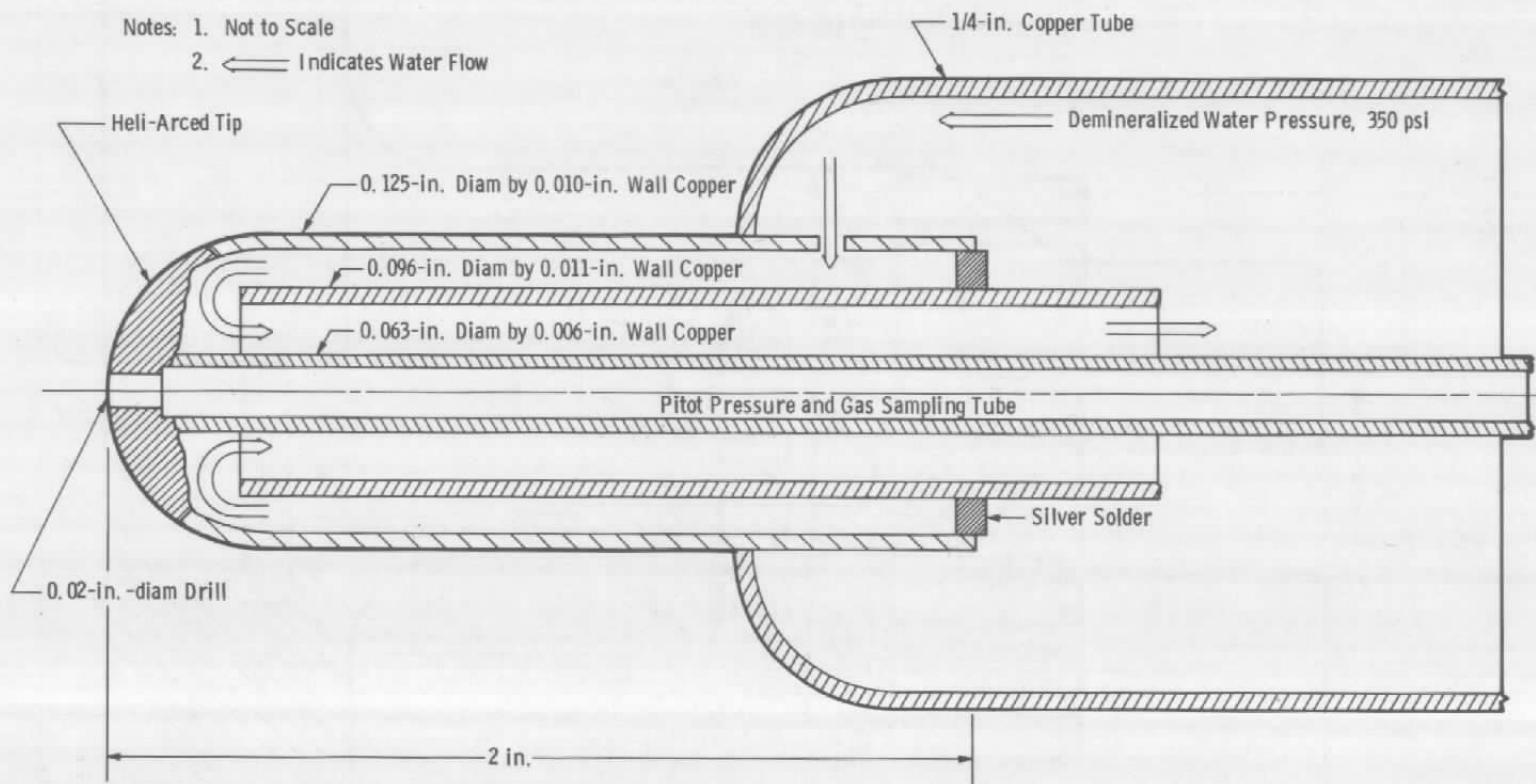
Figure 4. Water-cooled probe tip.

PM Tube

Collecting Optics

To Signal Conditioning Electronics

Flow

Probe
Volume

Beam Expander

Collimating Lens

2-D Bragg Cell

Argon
Laser

Beam
Reducer
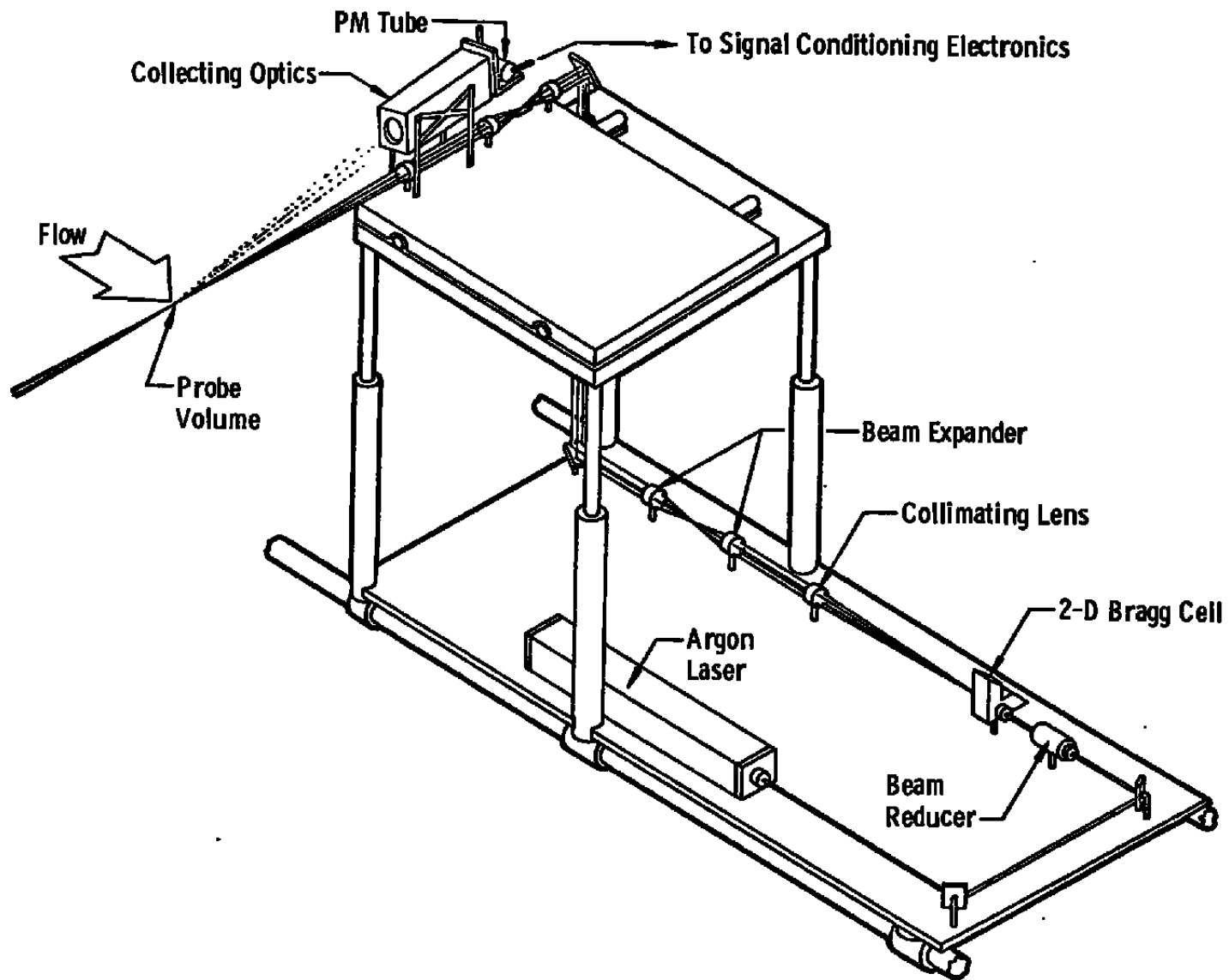
Figure 5. Laser velocimeter system.
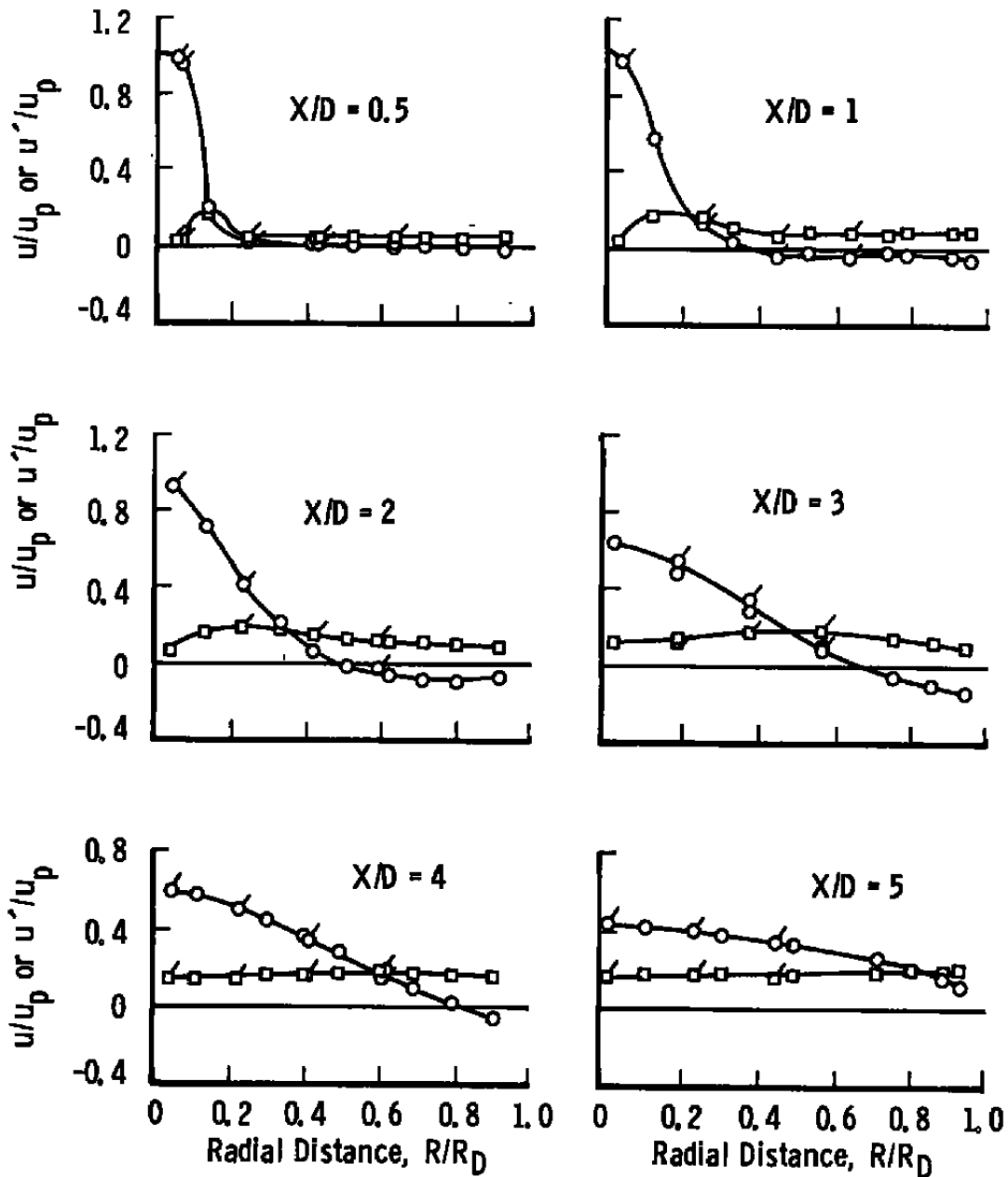
Figure 6. Radial distributions of mean axial velocities and
turbulence intensities, F/A = 0.143.
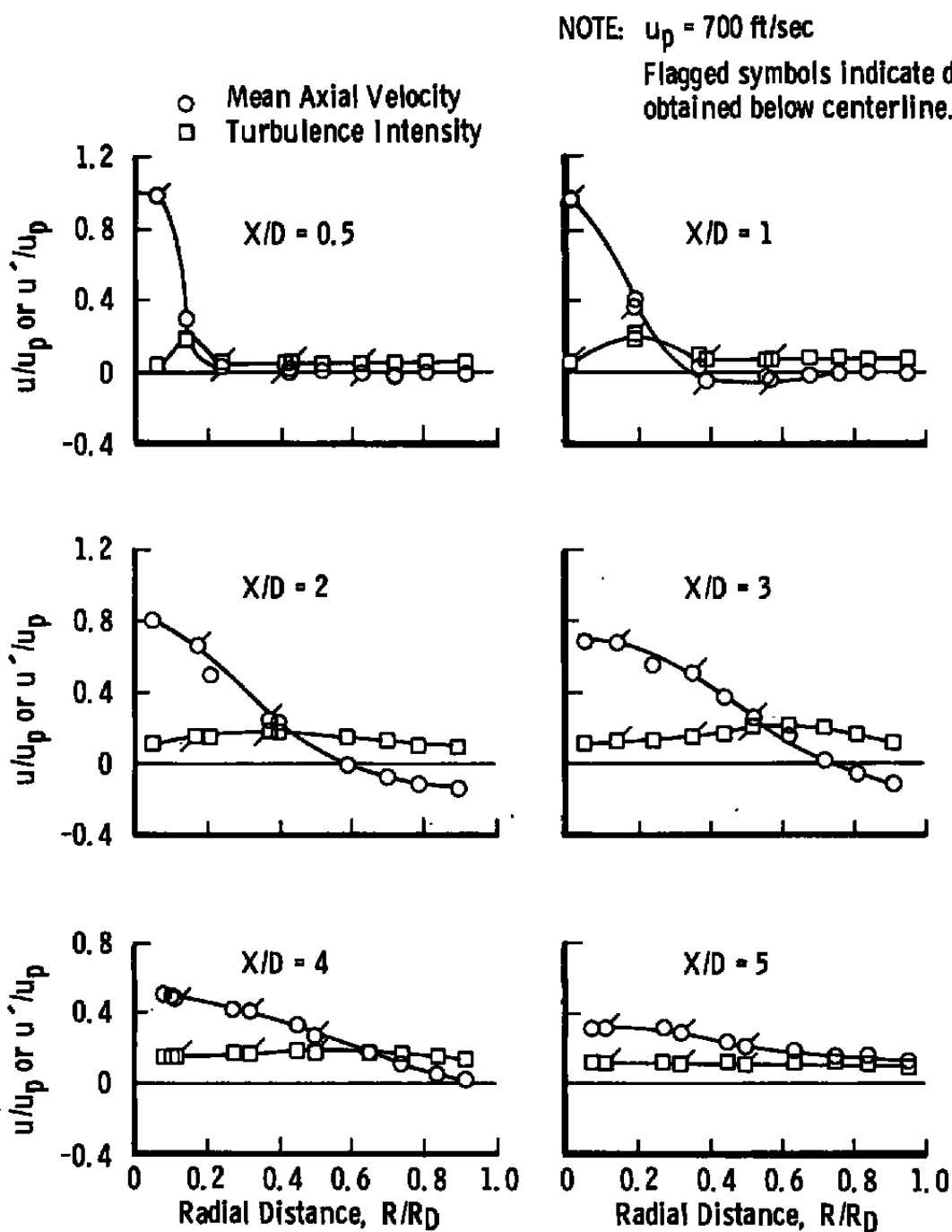
Figure 7. Radial distribution of mean axial velocities and turbulence intensities, F/A = 0.107.
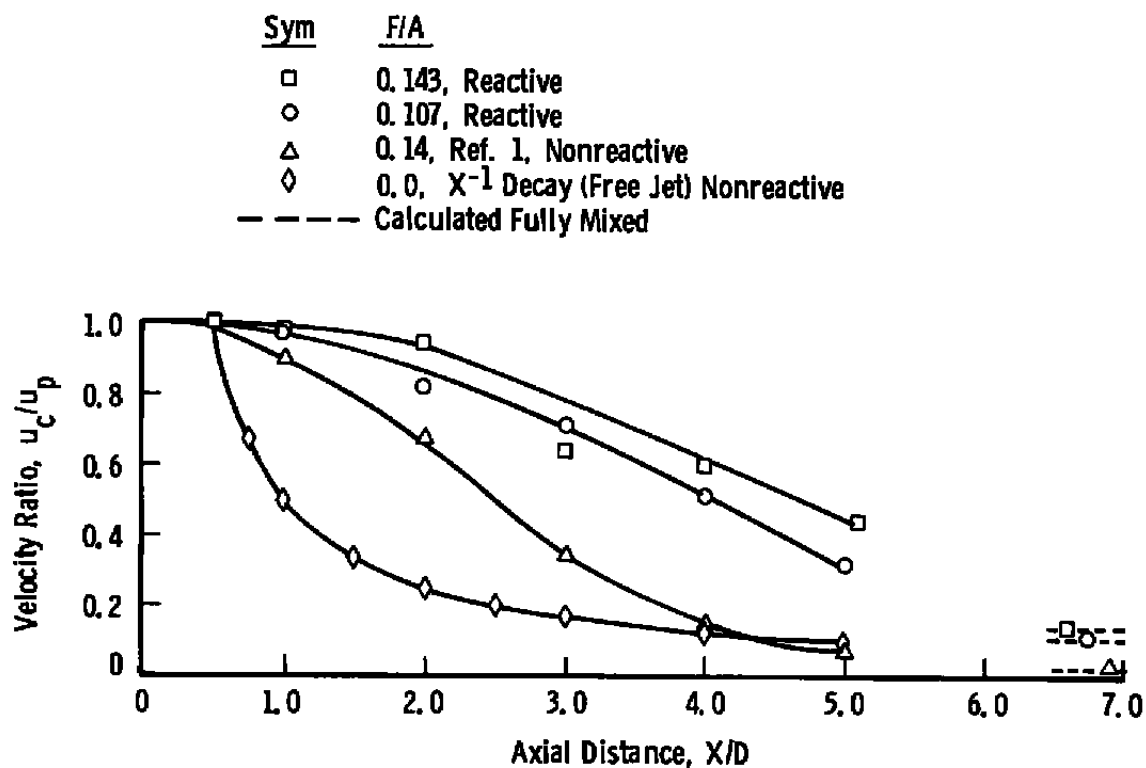
Figure 8. Axial distribution of centerline velocity.
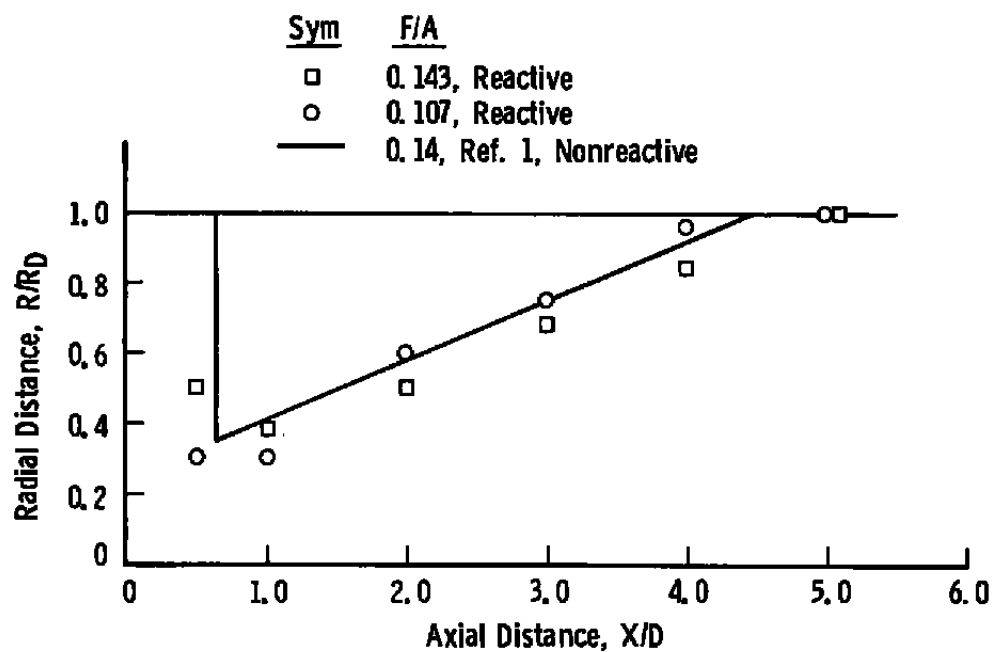
Figure 9. Location of points of zero mean axial velocity.

24
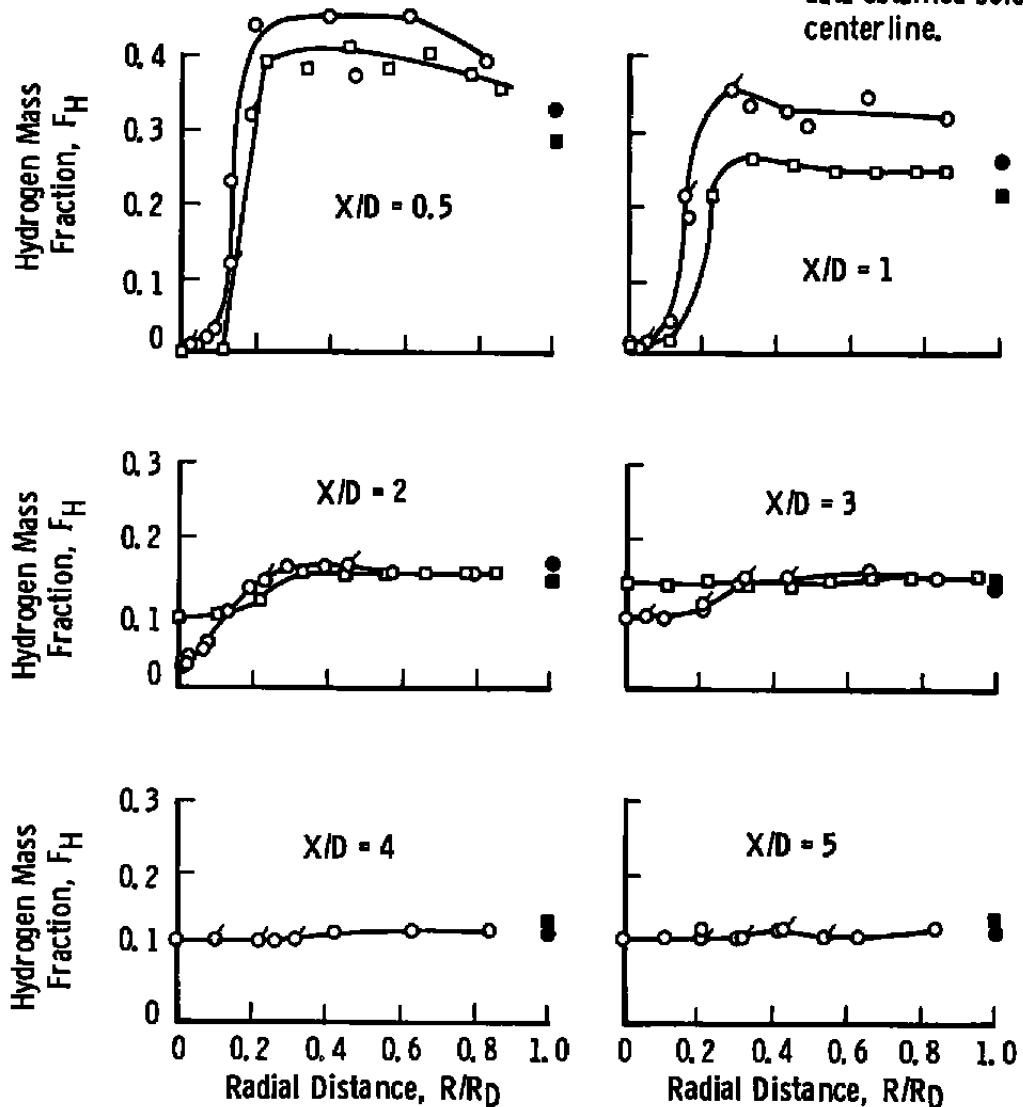
Figure 10. Radial distribution of hydrogen mass fraction, F/A = 0.143.
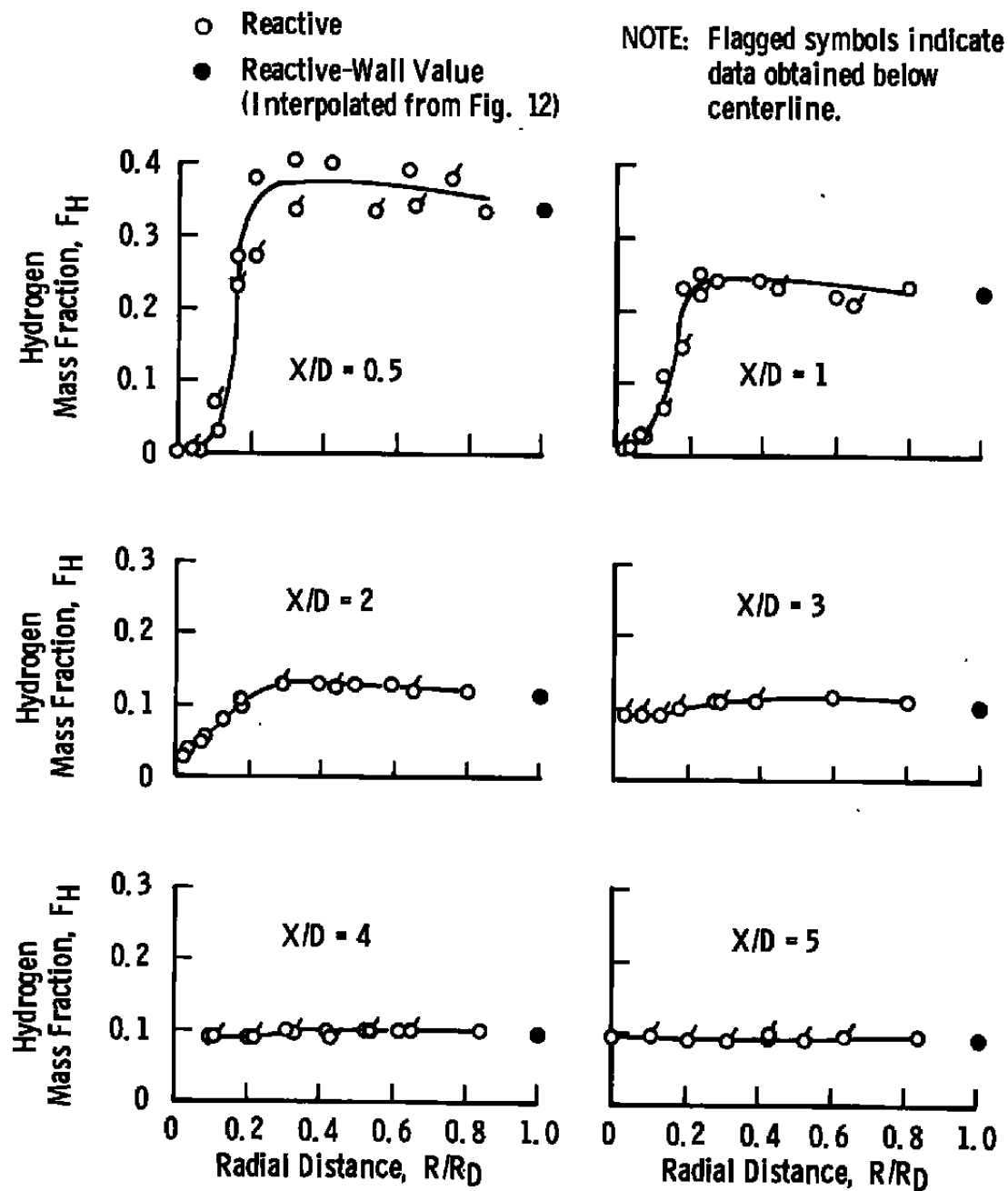
Figure 11. Radial distribution of hydrogen mass fraction, F/A = 0.107.
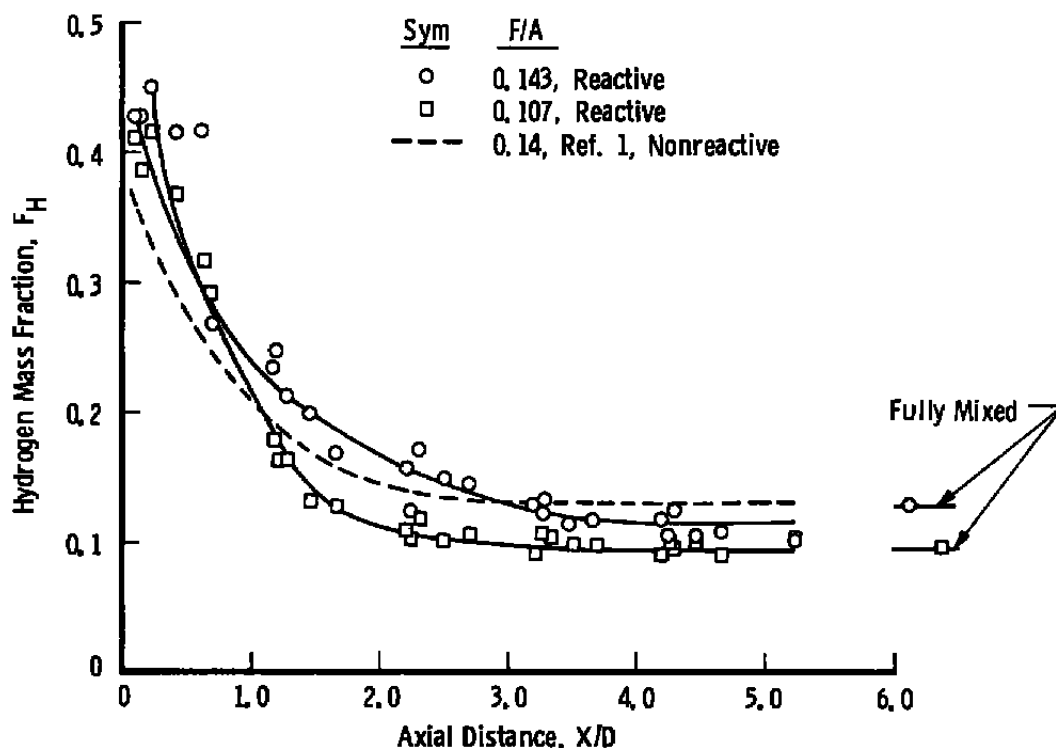
Figure 12. Axial distribution of hydrogen mass fraction, R/R_D = 1.0.
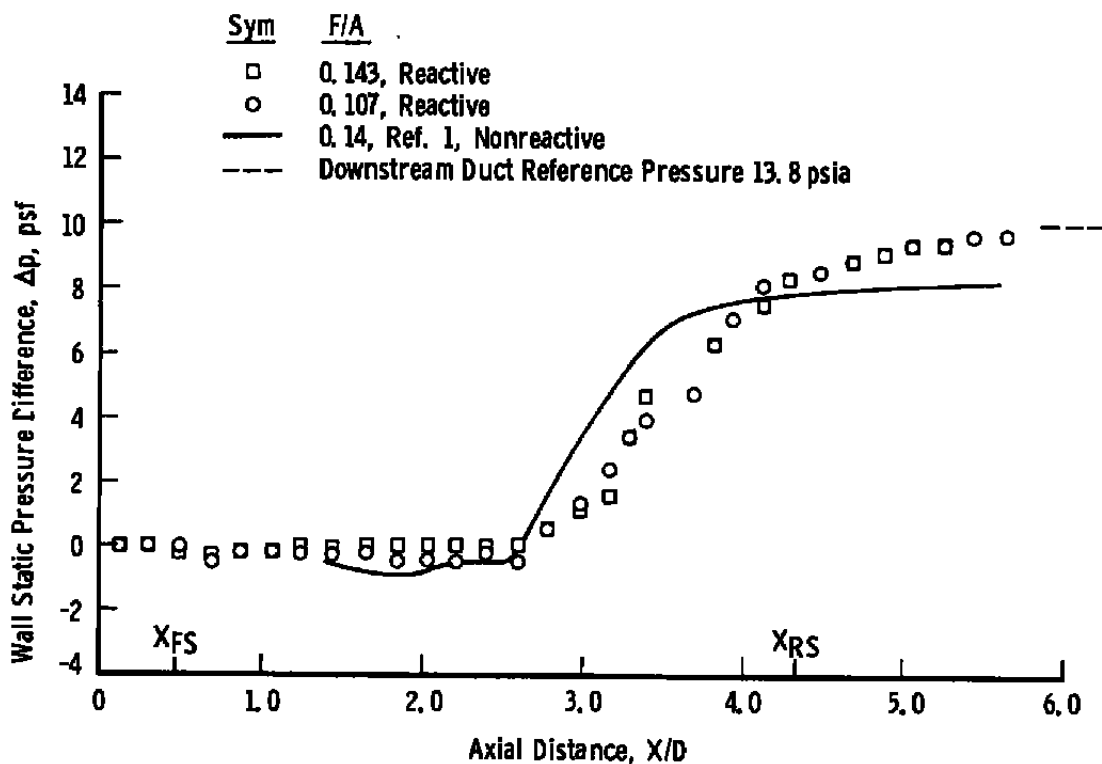
Figure 13. Axial distribution of wall static pressure.
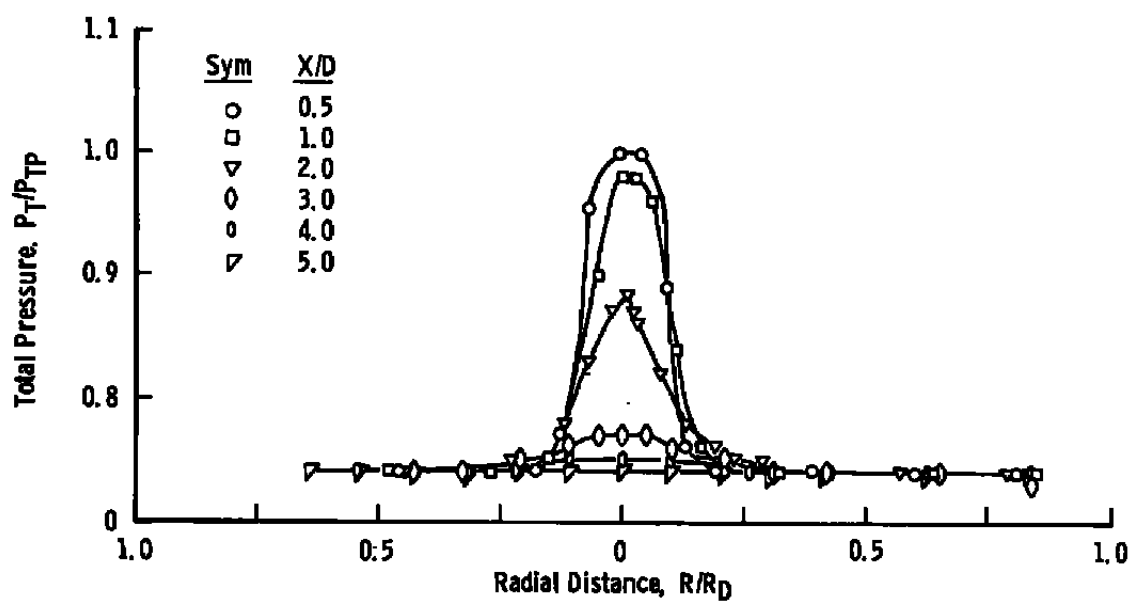
Figure 14. Radial distribution of total pressure, F/A = 0.143.
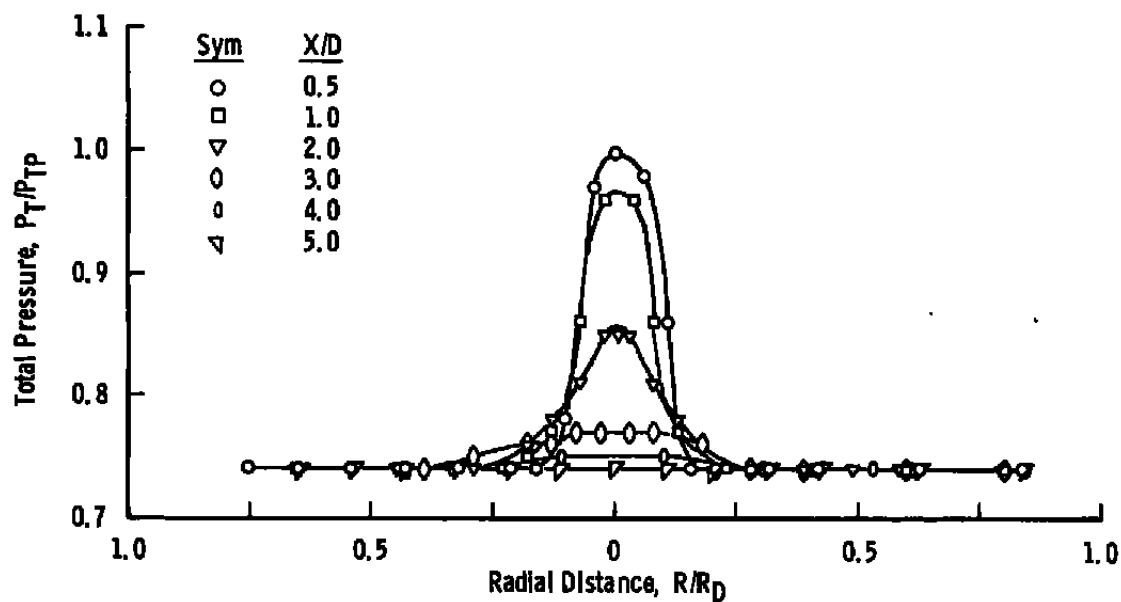
Figure 15. Radial distribution of total pressure, F/A = 0.107.
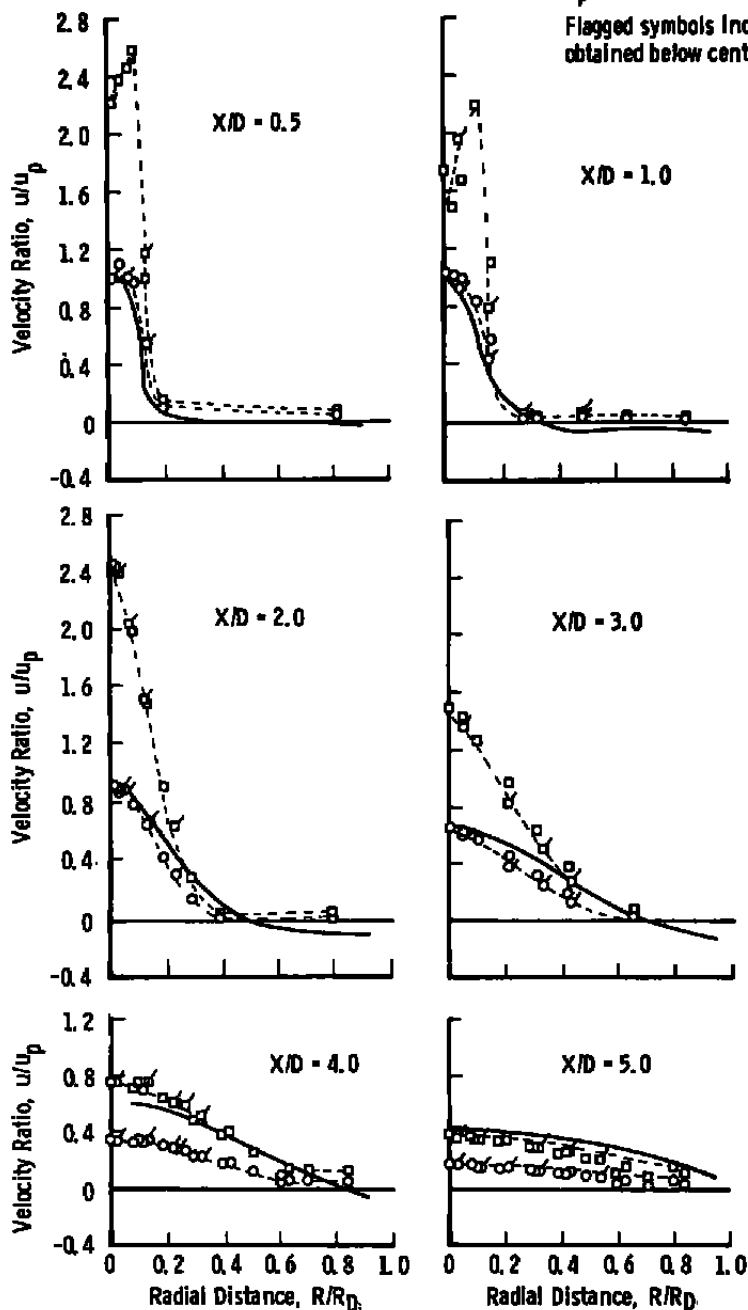
Figure 16. Comparison between measured and calculated velocities for frozen and equilibrium chemistry, F/A = 0.143.
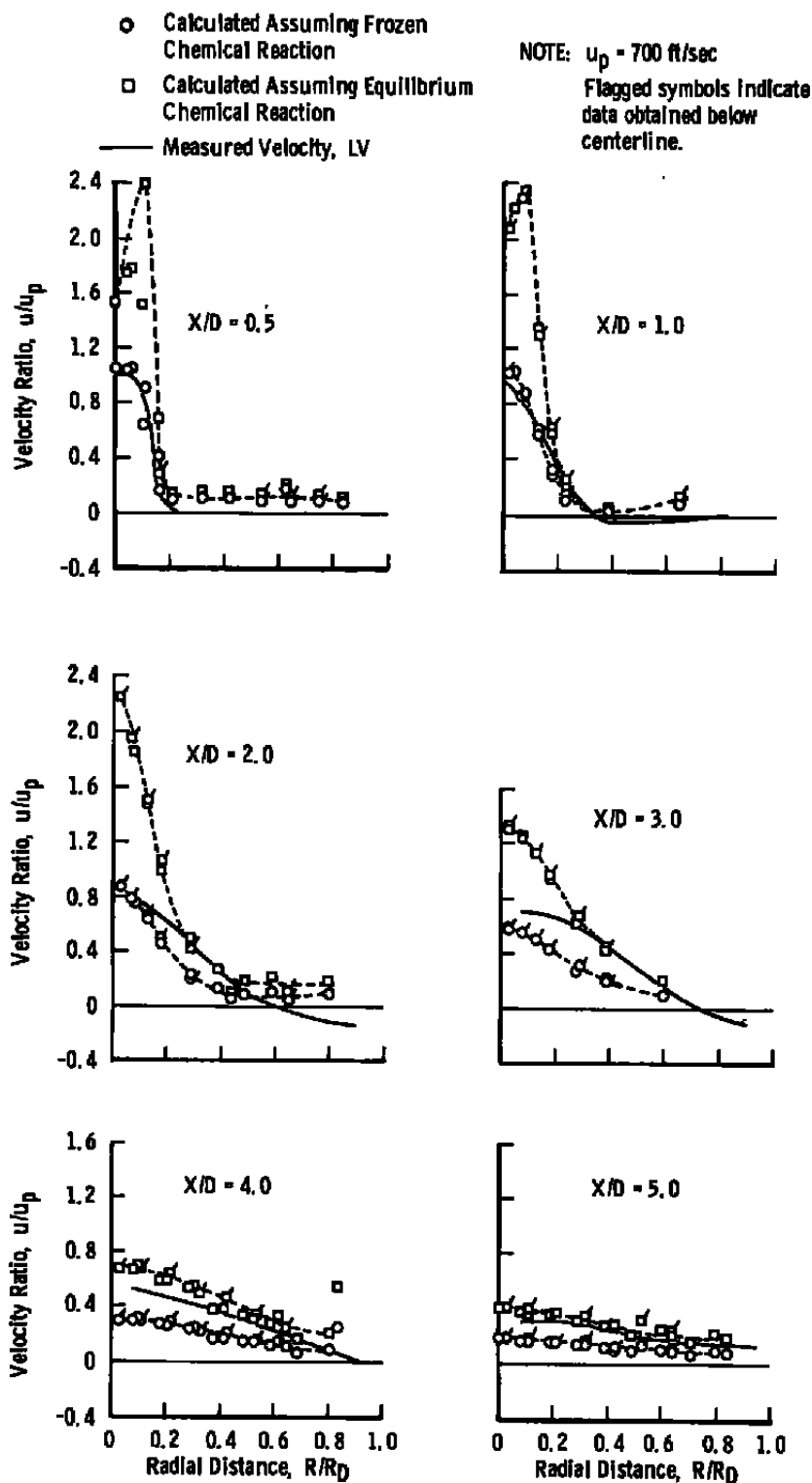
Figure 17. Comparison between measured and calculated velocities for frozen and equilibrium chemistry, F/A = 0.107.

Table 1. Uncertainties in Measured and Calculated Parameters, ϕ

Parameter Name and Symbol, ϕ	Characteristic Value of ϕ for Establishing the Uncertainty, ϕ_R	Precision Index, S_ϕ, percent of ϕ_R	Bias Limit, B_ϕ, percent of ϕ_R	Uncertainty $U_\phi = \pm(B_\phi + t_{95}S_\phi)$, percent of ϕ_R
Wall Static Pressure	0.04 psig	±2.0	±1.0	±5.0
Probe Pitot Pressure, High Range	3 psig	±1.0	±3.0	±5.0
Probe Pitot Pressure, Low Range	0.04 psig	±4.0	±8.0	±16.0
Wall Static Pressure for Velocity Calculations	0.04 psig	±4.0	±8.0	±16.0
Hydrogen Gas Concentrations, F_H, High Range	0.40	±2.0	±3.2	±7.2
Hydrogen Gas Concentrations, F_H, Low Range	0.05	±1.7	±1.7	±5.1
Primary Air Mass Flow	0.07 lbm/sec	±1.6	±3.5	±6.7
Secondary Hydrogen Mass Flow	0.01 lbm/sec	±1.6	±3.5	±6.7
Probe Radial Position	5 in.	±0.6	±5.0	±6.2
Axial Distance between Probe Tip and Nozzle Assembly	50 in.	±0.2	±1.0	±1.4
Calculated Velocity, High Range, Equilibrium Chemistry	700 ft/sec	±1.6	±3.3	±6.5
Calculated Velocity, Low Range, Equilibrium Chemistry	200 ft/sec	±2.8	±5.6	±11.2
Calculated Velocity, High Range, Frozen Chemistry	600 ft/sec	±0.5	±1.4	±2.4
Calculated Velocity, Low Range, Frozen Chemistry	100 ft/sec	±2.8	±5.4	±11.0

Table 2. Nominal Test Conditions

F/A	$\dot{w}_p$, lb/sec	$\dot{w}_s$, lb/sec	P_s, psia	T_T, °R	u_p, ft/sec (From LV)
0.143	0.075	0.011	13.8	530	700
0.107	0.075	0.008	13.8	530	700

APPENDIX A
EXPERIMENTAL DATA

Appendix A contains a tabulation of the experimental data obtained in the present study. The data include radial distributions of hydrogen mass fraction, mean axial velocity, turbulence intensity, and total pressure and axial distributions of wall hydrogen mass fraction and wall static pressure for the test conditions given in Table 2.

Table A-1. Mean Hydrogen Mass Fraction and Total Pressure, psi
a. F/A = 0.143

X/D = 0.5

R/R_D	0.81	0.60	0.39	0.19	0.13	0.09	0.04	-0.01
F_{H_2}	0.39	0.45	0.45	0.44	0.23	0.03	0.01	0.01
P_T	13.91	13.91	13.91	13.92	14.22	16.61	18.56	18.55

R/R_D	-0.07	-0.13	-0.18	-0.46
F_{H_2}	0.02	0.12	0.32	0.37
P_T	17.76	14.35	13.92	13.92

X/D = 1.0

R/R_D	0.85	0.54	0.42	0.32	0.21	0.16	0.11	0.06
F_{H_2}	0.31	0.34	0.32	0.33	---	0.18	0.04	0.01
P_T	13.77	13.78	13.77	13.78	13.84	14.16	15.71	17.89

R/R_D	0.03	0.00	-0.05	-0.15	-0.27	-0.48
F_{H_2}	0.003	0.01	0.01	0.21	0.35	0.30
P_T	18.26	18.27	16.98	13.98	13.60	13.79

X/D = 2.0

R/R_D	0.79	0.57	0.39	0.29	0.23	0.19	0.13	0.08
F_{H_2}	0.15	0.15	0.16	0.18	0.14	0.13	0.10	0.06
P_T	13.90	13.90	13.91	13.84	14.06	14.20	14.00	15.35

R/R_D	0.03	0.02	0.01	-0.02	-0.07	-0.12	-0.23	-0.45
F_{H_2}	0.04	0.04	0.03	0.03	0.05	0.09	0.14	0.16
P_T	16.12	16.32	16.37	16.26	15.46	14.66	14.05	13.92

X/D = 3.0

R/R_D	0.84	0.55	0.42	0.31	0.21	0.10	0.05	0.00
F_{H_2}	0.14	0.15	0.14	0.13	0.10	0.09	0.09	0.09
P_T	13.74	13.75	13.80	13.88	14.03	14.29	14.42	14.45

R/R_D	-0.05	-0.11	-0.21	-0.33	-0.43
F_{H_2}	0.09	---	0.11	0.14	0.14
P_T	14.37	14.24	13.98	13.84	13.79

X/D = 4.0

R/R_D	0.84	0.63	0.42	0.26	0.10	0.00	-0.11	-0.22
F_{H_2}	0.12	0.12	0.12	0.11	0.11	0.11	0.11	0.11
P_T	13.81	13.92	13.87	13.92	13.96	14.00	13.96	13.92

R/R_D	-0.32	---	-0.54
F_{H_2}	0.11	---	---
P_T	13.88	---	13.82

X/D = 5.0

R/R_D	0.84	0.63	0.42	0.31	0.21	0.10	0.00	-0.11
F_{H_2}	0.12	0.11	0.12	0.11	0.12	0.11	0.11	0.11
P_T	13.83	13.83	13.84	13.85	13.86	13.87	13.87	13.87

R/R_D	-0.21	-0.32	-0.43	-0.54	-0.64
F_{H_2}	0.11	0.11	0.12	0.11	---
P_T	13.87	13.86	13.84	13.82	13.82

Table A-1. Concluded
b. F/A = 0.107

X/D = 0.5

R/R_D	0.84	0.63	0.42	0.32	0.21	0.16	0.11	0.06
F_{H_2}	0.33	0.39	0.40	0.41	0.36	0.27	0.03	0.01
P_T	13.77	13.76	13.76	13.77	13.77	13.90	16.15	18.36
R/R_D	0.00	-0.04	-0.10	-0.16	-0.21	-0.32	-0.43	-0.54
F_{H_2}	0.003	0.01	0.07	0.23	0.27	0.33	---	0.33
P_T	18.49	18.18	14.57	13.81	13.77	13.77	13.76	13.78
R/R_D	-0.65	-0.75						
F_{H_2}	0.34	0.38						
P_T	13.76	13.78						

X/D = 1.0

R/R_D	0.80	0.60	0.39	0.28	0.23	0.18	0.13	0.08
F_{H_2}	0.23	0.22	0.24	0.24	0.25	0.23	0.11	0.03
P_T	13.85	13.85	13.85	13.85	13.86	13.97	14.41	16.14
R/R_D	0.04	-0.02	-0.07	-0.13	-0.18	-0.23	-0.44	-0.65
F_{H_2}	0.01	0.01	0.03	0.09	0.15	0.22	0.23	0.21
P_T	17.97	17.98	15.08	14.43	13.96	13.88	13.85	13.87

X/D = 2.0

R/R_D	0.60	0.58	0.49	0.39	0.29	0.18	0.13	0.08
F_{H_2}	0.12	0.13	0.13	0.13	0.13	0.11	0.08	0.06
P_T	13.83	13.84	13.85	13.85	13.90	14.15	14.51	15.06
R/R_D	0.03	0.01	-0.02	-0.07	-0.13	-0.18	-0.29	-0.44
F_{H_2}	0.04	0.03	0.03	0.05	0.08	0.10	0.13	0.13
P_T	15.82	15.90	15.85	15.23	14.59	14.20	13.93	13.86
R/R_D	-0.65							
F_{H_2}	0.12							
P_T	13.86							

X/D = 3.0

R/R_D	0.80	0.60	0.38	0.28	0.18	0.08	0.03	-0.03
F_{H_2}	0.11	0.12	0.11	0.11	0.10	0.09	0.09	0.08
P_T	13.86	13.87	13.91	13.98	14.12	14.35	14.41	14.47
R/R_D	-0.08	-0.13	-0.18	-0.29	-0.39			
F_{H_2}	0.09	0.09	0.10	0.11	0.11			
P_T	14.39	14.26	14.15	14.00	13.91			

X/D = 4.0

R/R_D	0.84	0.62	0.53	0.42	0.31	0.21	0.10	-0.08
F_{H_2}	0.10	0.10	0.10	0.10	0.10	0.09	0.09	---
P_T	13.86	13.82	13.83	13.84	13.88	13.91	13.95	---
R/R_D	-0.11	-0.22	-0.33	-0.43	-0.54	-0.65		
F_{H_2}	0.09	0.09	0.10	0.09	0.10	0.10		
P_T	13.95	13.91	13.86	13.84	13.83	13.81		

X/D = 5.0

R/R_D	0.84	0.64	0.43	0.32	0.21	0.11	0.00	-0.11
F_{H_2}	0.10	0.10	0.09	0.09	0.09	0.10	0.10	0.10
P_T	13.83	13.82	13.86	13.87	13.87	13.89	13.88	13.88
R/R_D	-0.21	-0.32	-0.43	-0.53	-0.64			
F_{H_2}	0.09	0.09	0.10	0.09	0.10			
P_T	13.88	13.86	13.85	13.84	13.82			

Table A-2. Mean Axial Velocity and Fluctuating Component, ft/sec
a. F/A = 0.143

X/D = 0.5

R/R_D	-0.92	-0.81	-0.71	-0.63	-0.53	-0.43	-0.42	-0.13
u	-13.0	-15.0	-8.0	-2.0	0.0	5.0	9.0	135.0
u'	36.0	33.0	32.0	33.0	34.0	33.0	32.0	119.0

R/R_D	0.05	0.06	0.24	0.43	0.83
u	895.0	673.0	17.0	12.0	12.0
u'	27.0	22.0	34.0	35.0	34.0

X/D = 1.0

R/R_D	-0.95	-0.80	-0.78	-0.73	-0.52	-0.32	-0.11	0.02
u	-40.0	-28.0	-19.0	-10.0	-24.0	24.0	413.0	689.0
u'	85.0	64.0	63.0	57.0	65.0	81.0	126.0	33.0

R/R_D	0.24	0.44	0.83
u	97.0	-29.0	-30.0
u'	122.0	54.0	55.0

X/D = 2.0

R/R_D	-0.92	-0.83	-0.72	-0.63	-0.52	-0.43	-0.34	-0.14
u	-50.0	-63.0	-58.0	-41.0	-8.0	48.0	148.0	507.0
u'	62.0	71.0	75.0	79.0	92.0	108.0	129.0	115.0

R/R_D	0.05	0.24	0.43	0.60
u	656.0	293.0	48.0	-24.0
u'	47.0	129.0	108.0	91.0

X/D = 3.0

R/R_D	---	-0.85	-0.86	-0.76	-0.57	-0.38	-0.18	-0.02
u	---	-96.0	-71.0	-37.0	61.0	202.0	349.0	450.0
u'	---	75.0	90.0	104.0	132.0	132.0	108.0	91.0

R/R_D	0.19	0.38	0.57
u	389.0	241.0	79.0
u'	94.0	125.0	136.0

X/D = 4.0

R/R_D	-0.92	-0.81	-0.71	-0.62	-0.51	-0.42	-0.32	-0.13
u	-40.0	17.0	72.0	127.0	203.0	263.0	320.0	409.0
u'	115.0	123.0	128.0	134.0	125.0	119.0	119.0	105.0

R/R_D	0.06	0.24	0.43	0.63
u	420.0	380.0	248.0	108.0
u'	103.0	104.0	122.0	128.0

X/D = 5.0

R/R_D	-0.95	-0.90	-0.82	-0.73	-0.51	-0.32	-0.12	0.02
u	86.0	115.0	144.0	190.0	240.0	279.0	299.0	314.0
u'	143.0	143.0	144.0	135.0	129.0	136.0	130.0	124.0

R/R_D	0.25	0.46
u	288.0	250.0
u'	125.0	119.0

Table A-2. Concluded
b. F/A = 0.107

X/D = 0.5

R/R$_D$	-0.92	-0.81	-0.72	-0.63	-0.52	-0.43	-0.42	-0.14
u	-8.0	-2.0	-4.0	3.0	4.0	6.0	8.0	216.0
u'	41.0	39.0	41.0	39.0	37.0	37.0	38.0	138.0

R/R$_D$	0.06	0.24	0.43	0.63
u	593.0	11.0	1.0	2.0
u'	33.0	38.0	36.0	38.0

X/D = 1.0

R/R$_D$	-0.95	-0.84	-0.76	-0.68	-0.56	-0.37	-0.19	0.01
u	-10.0	-4.0	-11.0	-15.0	-13.0	18.0	291.0	682.0
u'	55.0	48.0	55.0	53.0	54.0	75.0	129.0	35.0

R/R$_D$	0.19	0.38	0.57
u	254.0	-36.0	-33.0
u'	139.0	51.0	47.0

X/D = 2.0

R/R$_D$	---	-0.90	-0.79	-0.70	-0.59	-0.40	-0.21	-0.05
u	---	-87.0	-77.0	-48.0	1.0	167.0	351.0	572.0
u'	---	67.0	79.0	95.0	113.0	125.0	110.0	81.0

R/R$_D$	0.17	0.37	0.55
u	466.0	177.0	-15.0
u'	111.0	136.0	92.0

X/D = 3.0

R/R$_D$	---	-0.91	-0.81	-0.72	-0.62	-0.44	-0.24	-0.05
u	---	-83.0	-38.0	13.0	111.0	261.0	395.0	484.0
u'	---	85.0	117.0	140.0	151.0	119.0	94.0	82.0

R/R$_D$	0.14	0.35	0.52
u	478.0	356.0	204.0
u'	88.0	108.0	143.0

X/D = 4.0

R/R$_D$	---	---	-0.92	-0.84	-0.75	-0.65	-0.45	---
u	---	---	15.0	39.0	82.0	127.0	230.0	---
u'	---	---	82.0	109.0	118.0	127.0	131.0	---

R/R$_D$	-0.27	-0.10	-0.08	0.11	0.32	0.50
u	294.0	349.0	361.0	342.0	286.0	186.0
u'	117.0	107.0	105.0	109.0	117.0	123.0

X/D = 5.0

R/R$_D$	---	-0.95	---	-0.84	-0.75	-0.64	-0.45	-0.27
u	---	92.0	---	99.0	110.0	126.0	157.0	215.0
u'	---	66.0	---	72.0	78.0	84.0	87.0	86.0

R/R$_D$	-0.07	0.11	0.32	0.50
u	219.0	217.0	198.0	151.0
u'	86.0	85.0	79.0	82.0

Table A-3. Hydrogen Mass Fraction at the Wall

F/A = 0.143		F/A = 0.107	
X/D	F_H	X/D	F_H
0.143	0.428	0.143	0.411
0.170	0.427	0.170	0.386
0.260	0.450	0.260	0.416
0.450	0.416	0.450	0.368
0.650	0.416	0.650	0.316
0.720	0.267	0.720	0.292
1.19	0.234	1.19	0.179
1.22	0.247	1.22	0.164
1.29	0.212	1.29	0.164
1.48	0.199	1.48	0.132
1.67	0.169	1.67	0.127
2.22	0.156	2.22	0.108
2.24	0.129	2.24	0.101
2.31	0.171	2.31	0.118
2.51	0.149	2.51	0.101
2.70	0.144	2.70	0.105
3.20	0.128	3.22	0.092
3.27	0.123	3.27	0.106
3.29	0.133	3.32	0.104
3.48	0.114	3.51	0.099
3.67	0.117	3.70	0.098
4.20	0.118	4.20	0.089
4.25	0.105	4.27	0.099
4.29	0.125	4.29	0.096
4.48	0.105	4.48	0.099
4.68	0.109	4.68	0.090
5.25	0.102	5.25	0.103

Table A-4. Wall Static Pressure Distribution

	F/A = 0.143	F/A = 0.107		F/A = 0.143	F/A = 0.107
X/D	Δp, psf	Δp, psf	X/D	Δp, psf	Δp, psf
0.12	0	0	3.17	1.56	2.34
0.31	0	0	3.29	3.38	3.38
0.50	-0.26	0	3.41	4.68	3.90
0.69	-0.26	-0.52	3.71	---	4.68
0.88	-0.26	-0.26	3.83	6.24	6.24
1.07	-0.26	-0.26	3.94	---	7.02
1.26	0	-0.26	4.13	7.54	8.06
1.46	0	-0.26	4.32	8.32	---
1.65	0	-0.26	4.51	---	8.58
1.84	0	-0.52	4.70	8.84	8.84
2.03	0	-0.52	4.89	9.1	---
2.22	0	-0.52	5.08	9.36	9.36
2.41	0	-0.26	5.27	9.36	9.36
2.60	0	-0.52	5.46	---	9.62
2.79	0.52	0.52	5.65	---	9.62
2.98	1.04	1.30			

APPENDIX B
CHEMISTRY MODEL

R. P. Rhodes

In order to calculate free-stream gas properties in a potentially reacting system from total pressure, static pressure, and gas composition, the following assumptions were made:

1. There is a unique relationship between elemental composition and total enthalpy. In this analysis, both gases were introduced near room temperature where H_T is 0 and all mixtures were assumed to have an H_T of 0; H_T is defined by:

$$H_T = \sum_i \left[\beta_i \left(\int_{T_r}^{T} C_{p_i} \, dT + H_{f_r} \right) \right] + u^2/2 \tag{B-1}$$

where

β_i = the moles/g of species i

C_{p_i} = The molar specific heat of species i

T = Static temperature

u = Velocity

T_r = Reference temperature for the enthalpy

H_f = Heat of formation of species i

2. The state of reaction is known. Calculations were made assuming both frozen (unreacted) and equilibrium (completely reacted) gases.

3. The compression process from the free stream to stagnation pressure on the probe tip is isentropic and chemically frozen.

4. Composition of air is assumed to be 0.2095 mole fraction O_2 and 0.7905 mole fraction N_2.

5. The static pressure is assumed constant with duct radius and equal to the measured wall value.

6. The gas mixtures are thermally perfect.

41

Given the pressure, enthalpy, and chemical composition, the computer program of Ref. 11 was used to calculate the gas properties. The program may be run assuming either frozen chemistry, in which case the species partial pressures are required, or equilibrium chemistry using the molar ratios of the elements.

The gas properties are calculated by the following procedure:

1. From the mass fraction of elemental hydrogen, compute the moles/unit mass of each element,

$$\beta_H = \alpha_H / 1.008$$

$$\beta_O = 0.2095 (1 - \alpha_H) / 16 \qquad \text{(B-2)}$$

$$\beta_N = 0.7905 (1 - \alpha_H) / 14.008$$

These variables are input to the gas properties program for the equilibrium calculation. For the frozen calculation, the partial pressures of H_2, O_2, and N_2 are required. For the gas constituents being considered, the moles/unit mass (β) of the molecules is $1/2\ \beta$ of the element, and:

$$P_{P_i} = P \beta_i / \sum_i \beta_i \qquad \text{(B-3)}$$

where i is each species.

2. A velocity is assumed and the static enthalpy is calculated from:

$$H = H_T - u^2/2 \qquad \text{(B-4)}$$

3. The remaining free-stream properties including entropy (S_2) are calculated from the free-stream enthalpy, the measured static pressure, and composition using the gas properties program described in Ref. 9.

4. An estimate of the total pressure is obtained from the isentropic relationship:

$$P_{T_1} = P \left(1 + \frac{\gamma - 1}{2} M^2 \right)^{\gamma/(\gamma-1)} \qquad \text{(B-5)}$$

using the Mach number and γ from the calculations in Eq. (B-3). The entropy (S_1) is then calculated using the gas properties program with frozen composition, P_T from Eq. (B-5), and H_T. Since, for an adiabatic system,

$$P_{T_2}/P_{T_1} = \text{Exp}.[-(S_2 - S_1)\,W/R_g] \tag{B-6}$$

the total pressure P_{T2} corresponding to the isentropic compression at S_2 may be obtained from Eq. (B-6).

5. Steps 2 to 4 are repeated with a new value of u obtained from $(u_{new} - u_{old}) \sim (P_{T_{measured}} - P_{T_{old}})/(\rho u)_{old}$ until $(u_{new} - u_{old})$ is less than 1 ft/sec. The gas properties obtained in step 3 on the final iteration are taken to be the free-stream properties.

NOMENCLATURE

A   Mass flow rate of air, lbm/sec

B_Φ Bias of the parameter (Φ), unit of Φ

C_p Specific heat at constant pressure, Btu/mole-°R

D   Duct diameter, 5.24 in.

F   Mass flow rate of fuel (hydrogen), lbm/sec

F_H Hydrogen mass fraction, total Hydrogen mass/total mass

H   Enthalpy, Btu/lb

H_{f_i} Heat of formation of species i, Btu/lbm

M   Mach number

N_{Re} Reynolds number, based on primary jet radius

P   Pressure, psfa

P_{p_i} Partial pressure of species i, psfa

Δp Difference between wall static pressure at station X and station zero, psf

R   Radius, in.

R_g Universal gas constant 1,545 ft-lbf/lb$_{mole}$-°R

S   Entropy Btu/lbm-°R

S_Φ Precision index of the parameter, units of Φ

T   Temperature, °R

U_Φ Uncertainty in the parameter, units of Φ

u   Mean axial velocity, ft/sec

u'   Root-mean-square fluctuating velocity, ft/sec

u'/u_p Axial turbulence intensity

W   Molecular weight of the mixture, lbm/mole

$\dot{w}$ Mass flow, lbm/sec

X Axial coordinate measured from primary nozzle exit location, in.

X_{FS} Axial location of the forward stagnation point on the duct wall (Fig. 1)

X_{RS} Axial location of the rear stagnation point on the duct wall (Fig. 1)

a_H Mass fraction of elemental hydrogen

β_i Parameter, moles/gm of species i

γ Ratio of specific heats

μ Dynamic viscosity, lbm/ft-sec

ξ Measured parameter which defines Φ

ρ Density, lbm/ft^3

Φ Dummy parameter, scalar

SUBSCRIPTS

1,2   Arbitrary stations in iteration scheme

A   Argon

c   Centerline

D   Duct

H   Hydrogen

i   Arbitrary chemical species

N   Nitrogen

O   Oxygen

p   Primary jet property

r   Reference value

s   Secondary

T   Total or stagnation conditions